Master's thesis

NTNU
Norwegian University of Science and Technology
Faculty of Engineering
Department of Structural Engineering

Vidar Goldfine

Structural Monitoring of Norsenga Bridge

Master's thesis in Civil and Environmental Engineering
Supervisor: Ole Øiseth
Co-supervisor: Davide Raviolo
December 2023

NTNU
Norwegian University of
Science and Technology

Vidar Goldfine

Structural Monitoring of Norsenga Bridge

Master's thesis in Civil and Environmental Engineering
Supervisor: Ole Øiseth
Co-supervisor: Davide Raviolo
December 2023

Norwegian University of Science and Technology
Faculty of Engineering
Department of Structural Engineering

NTNU
Norwegian University of
Science and Technology

Abstract

After the 2022 Tretten Bridge collapse, numerous timber bridges in Norway faced closure and structural reassessment due to suspected issues. Among these, the Norsenga Bridge underwent scrutiny by the Norwegian Road Administration, which initiated a Structural Health Monitoring (SHM) campaign. SHM employs sensors to continuously assess structures, detect defects, and predict issues to ensure ongoing safety by understanding structural integrity and behavior. This study focuses on comprehending the Norsenga Bridge's structural behavior, utilizing vibration data from the SHM system and a newly developed finite element model of the structure.

To this extent, the research computes theoretical natural frequencies and mode shapes through an ABAQUS-built FE model. In addition, system identification via frequency domain decomposition (FDD) and covariance-driven stochastic subspace identification (Cov-SSI) has been performed with the experimental data, consisting of measured accelerations at several bridge locations. Significant discrepancies between the initial FE model and the experimental responses prompted a manual finite element model updating (FEMU) procedure to enhance accuracy, accounting for the bridge's dynamic behavior. Additionally, simulated damages were introduced to assess their impact on the bridge's numerical dynamic response.

Accurately modeling the bridge's dynamic response poses several challenges. Notably, modeling the joints in the trusses, considered fixed in the proposed FE model, is likely a source of significant error, artificially inflating overall stiffness and impeding accurate response predictions. Moreover, as per the FE model, the bridge's static indeterminacy limited substantial observable changes in the numerical response post-damage, underscoring inherent complexities in its analysis.

Sammendrag

Etter kollapsen på Tretten bru i 2022 stod flere trebroer i Norge i fare for stenging og strukturell gjennomgang på grunn av mistenkte problemer. Blant disse ble Norsenga bru gjennomgått av Statens vegvesen, som igangsatte en kampanje for strukturhelseovervåking (SHM). SHM bruker sensorer for å kontinuerlig evaluere konstruksjoner, identifisere feil og forutse mulige problemer for å sikre løpende sikkerhet ved å forstå strukturell integritet og oppførsel. Denne oppgaven fokuserer på å forstå Norsenga bru sin strukturelle oppførsel ved å bruke vibrasjonsdata fra SHM-systemet og en nyutviklet endelig elementmodell (FE-modell) av strukturen. Studien innebærer beregning av teoretiske naturlige frekvenser og modusformer ved bruk av en FE-modell bygget i ABAQUS. I tillegg ble systemidentifikasjon ved hjelp av frekvensdomene-dekomponering (FDD) og kovariansdrevet stokastisk underromsidentifikasjon (Cov-SSI) utført basert på målte akselerasjoner på flere brolokasjoner.

Betydelige forskjeller mellom den opprinnelige FE-modellen og de eksperimentelle responsene nødvendiggjorde en manuell prosess for oppdatering av endelig elementmodell (FEMU) for å forbedre nøyaktigheten, med tanke på broens dynamiske oppførsel. Dessuten ble simulerte skader introdusert for å vurdere deres innvirkning på broens numeriske dynamiske respons.

Å nøyaktig modellere broens dynamiske respons innebærer flere utfordringer. Særlig modelleringen av knutepunktene i fagverket, som ble ansett som fast innspente i den foreslåtte FE-modellen, antas å introdusere betydelig feil ved å kunstig øke den samlede stivheten og hindre nøyaktige responsprognoser. Videre, basert på FE-modellen, begrenset broens statiske indeterminasjon betydelige endringer i den numeriske responsen etter skade, noe som understreker de iboende kompleksitetene i analysen.

Contents

List of Figures

List of Tables

1 Introduction

Figure 1: Norsenga Bridge viewed from the south

Norsenga Bridge is a 94.5-meter-long timber truss bridge on E16 in Kongsvinger, crossing over a railway, as shown in Figure 1. The construction of the bridge ended in 2017. It is one of 14 timber truss bridges that were temporarily closed due to the collapse of Tretten Bridge on 15. August 2022[1]. Norsenga was partly reopened 15. September 2022. It remains only open for one-way traffic, due to potential issues found with the structure.

The object of the report is to initialize an effort to deploy structural monitoring of Norsenga Bridge, which will later evolve into continuous structural health monitoring (SHM).

This report will cover the creation and choices made for a Finite Element model (FE model) of Norsenga bridge, the instrumentation of the actual bridge, the system identification (SI), and the comparison between the numerical dynamic results of the FE model to the system identification results. To increase the model's ability to accurately represent the dynamic behavior of the bridge, the model is manually updated to resemble the results from the system identification. Using the updated model, damages are introduced to study their impact on the model's structural response and to assess their detectability through changes in modal parameters (natural frequencies and mode shapes).

2 Theoretical Background

This report is focused on analyzing the dynamic behavior of Norsenga Bridge. For this purpose, the theoretical background of the Finite Element Method (FEM), the two methods of System Identification: frequency domain decomposition (FDD) and Covariance-Driven Stochastic Subspace Identification (SSI), the method of comparison: modal assurance criterion (MAC), the theory behind updating the FE model, and background for structural health monitoring will all be presented here. In order to properly explain these techniques, general dynamic theory will also be introduced.

2.1 Natural Frequency of Single Degree Of Freedom (SDOF) System

Describing the dynamic behavior of a system involves identifying its natural frequencies and the associated mode shapes[2]. Initially, the natural frequency for a single degree of freedom (SDOF) system will be established. Subsequently, the focus will shift to determining the natural frequencies of the multi-degree of freedom (MDOF) system. From the MDOF system corresponding mode shapes can be revealed. The equation of motion for a single degree of freedom system is given by:

$$m\ddot{u} + c\dot{u} + ku = F(t) \tag{1}$$

where m, c, k, u, and F(t) represent the mass, damping, stiffness, displacement, and time-varying external force acting on the system, respectively. The natural frequency denotes the system's frequency of free vibration when F(t) = 0. The undamped natural frequency, primarily determined by the stiffness and mass, is mathematically expressed as:

$$\omega_n = \sqrt{k/m} \tag{2}$$

For any real-life system, there will be damping. Damping reduces the speed and displacement of the system. The damping ratio is given by:

$$\zeta = c/c_{cr} \tag{3}$$

and the damped natural frequency is given by:

$$\omega_d = \omega_n\sqrt{1-\zeta^2} \tag{4}$$

Typically, the anticipated damping ratio for a system is rarely above 5%, and it generally doesn't significantly affect the natural frequency. Any resulting impact on the natural frequency is usually marginal, leading to only a slight reduction. Consequently, in many cases, the calculation of the natural frequency often disregards the influence of damping.

2.2 Natural Frequency and Mode Shapes of Multi Degree Of Freedom (MDOF) System

A multi-degree-of-freedom system often discretizes a more complex system[2]. The MDOF system can be described similarly to the SDOF system, where the equation of motion is given by:

$$\mathbf{M}\ddot{\boldsymbol{u}} + \mathbf{C}\dot{\boldsymbol{u}} + \mathbf{K}\boldsymbol{u} = \mathbf{F}(t) \tag{5}$$

as in Equation 1, where **M, C, K, u** and **F**(t) is the mass matrix, damping matrix, stiffness matrix, displacement vector and load vector. Again, the impact of damping on the natural frequencies remains minimal. Therefore, disregarding damping allows for the determination of natural frequencies by solving the eigenvalue problem:

$$det[\mathbf{K} - \omega_n^2\mathbf{M}] = \mathbf{0} \tag{6}$$

Consequently, there is an amount of natural frequencies and Degrees of Freedom (DOFs) within the system. Each of these frequencies corresponds to a specific mode shape that the structure will exhibit when stimulated by that particular frequency. These mode shapes are obtained by solving the following equation:

$$[\mathbf{K} - \omega_n^2\mathbf{M}]\phi_n = \mathbf{0} \tag{7}$$

where ϕ is the mode shape vector containing the relative displacement of the DOFs in the n_{th} natural frequency.

2.3 Finite Element Analysis

The finite element method stands as a formidable tool in the realm of structural engineering. It involves the discretization of structures into nodes and elements to provide numerical solutions. Utilizing this approach, the stiffness matrix **K** and mass matrix **M** are constructed. As demonstrated in Equations 6 and 7, these matrices facilitate the determination of natural frequencies and their corresponding mode shapes. However, it's important to note that the discretization process also impacts the representation of mode shapes. If the structure is inadequately discretized, higher-order mode shapes may be insufficiently represented.

2.4 Cross Correlation Matrix

When examining stochastic signals, our focus lies in understanding the characteristic variations of the signal across time. This vital information is encapsulated within the auto-correlation function[3]. For a stochastic signal, the auto-correlation function is defined as the anticipated value of the signal multiplied by itself at a certain time lag.

$$R_{xx} = E[x(t) * x(t+\tau)] \tag{8}$$

The decay rate provides insight into the duration for which the signal maintains correlation with itself.

Likewise, the cross-correlation function is defined in a similar manner, representing the anticipated value of one stochastic signal multiplied by another stochastic signal at a specific time lag.

$$R_{xy} = E[x(t) * y(t+\tau)] \tag{9}$$

The auto- and cross correlation functions are symmetric about the y-axis and go to zero.

The cross correlation matrix contains both the auto correlation function and cross correlation function of all its signals. For a 2x2 matrix, it is given by

$$\mathbf{R}_{xy} = \begin{bmatrix} R_{xx} & R_{xy} \\ R_{yx} & R_{yy} \end{bmatrix} \tag{10}$$

2.5 Cross Spectral Density Matrix

To ascertain the frequency composition of a signal, employing the Fourier transform directly on the signal itself isn't viable due to its infinite extent. Hence, a function with a finite span is necessary. Given that both the auto- and cross-correlation functions converge to zero, utilizing the Fourier transform on these functions gives the auto- and cross-spectral densities[3]. The auto-spectral density is expressed as:

$$S_{xx}(\omega) = 1/2\pi * \int_{-\infty}^{\infty} R_{xx}(\tau) * e^{-i\omega\tau}\, d\tau \tag{11}$$

and the cross spectral density is given by

$$S_{xy}(\omega) = 1/2\pi * \int_{-\infty}^{\infty} R_{xy}(\tau) * e^{-i\omega\tau}\, d\tau \tag{12}$$

The cross spectral density matrix contains the auto- and cross spectral densities of all its signals. For a 2x2 matrix, it is given by

$$\mathbf{S}_{xy} = \begin{bmatrix} S_{xx} & S_{xy} \\ S_{yx} & S_{yy} \end{bmatrix} \tag{13}$$

For structural dynamics, the signal can represent the load the structure is subjected to or the response of the structure.

2.6 Frequency Domain Decomposition (FDD)

If a finite element model is not provided, it is possible to estimate the modal properties from measurements of structural responses. Doing this is called system identification. One method of system identification is called Frequency Domain Decomposition[4].

Provided a recording of acceleration, the cross-spectral density matrix $\mathbf{S}_{xy}$ is approximated using Welsh's method. Welsh's method divides a recording into several smaller parts, possibly overlapping, and calculates a cross-spectral density matrix for each part. These are averaged to approximate the cross-spectral density matrix of the system response.

FDD is based on the singular value decomposition (SVD) of the cross-spectral density matrix. The SVD is widely utilized in linear algebra. It factorizes the matrix $\mathbf{M}$ as follows:

$$\mathbf{M} = \mathbf{U}\mathbf{\Sigma}\mathbf{V}^H \tag{14}$$

where H denotes the Hermittian transpose (transpose and complex conjugation). $\mathbf{\Sigma}$ is a diagonal matrix, with the singular values σ_i. Singular values are real. $\mathbf{U}$ is a matrix containing the left singular vectors $\mathbf{u}_i$. These vectors can be complex if $\mathbf{M}$ is complex. Simply put, $\mathbf{M}$ is constructed from many singular vectors, and the singular values describe the importance of the corresponding singular vectors.

In dynamics, the physical response can be expressed as the sum of all contributions from the modes as follows:

$$\mathbf{x}(t) = \boldsymbol{\phi}\eta(t) \tag{15}$$

The spectrum of the response can be expressed as follows:

$$\mathbf{S}_x(\omega) = \Phi\mathbf{S}_\eta(\omega)\Phi^H \tag{16}$$

For natural frequencies, one mode will dominate the total response due to resonance. Considering this, the spectral matrix can be approximated by only considering the first singular vector as follows:

$$\mathbf{S}_x(\omega_s) \approx \mathbf{u}_1\boldsymbol{\sigma}_1\mathbf{v}_1^H \tag{17}$$

The mode shape $\boldsymbol{\phi}_s$ is then approximately:

$$\boldsymbol{\phi}_s = \mathbf{u}_1 \tag{18}$$

$\boldsymbol{\phi}_s$ i complex.

2.7 Covariance-Driven Stochastic Subspace Identification (SSI)

Covariance-Driven Stochastic Subspace Identification is a comprehensive method of system identification. Only the most important details of the applied implementation are mentioned here.

The block-Handel matrix is the starting point of the analysis[5], which is constructed by sub-matrices representing the channels l, of the measurements, with varying time shifts as follows:

$$\mathbf{H}_i = \begin{bmatrix} \mathbf{R}_1 & \mathbf{R}_2 & ... & \mathbf{R}_i \\ \mathbf{R}_2 & \mathbf{R}_3 & ... & \mathbf{R}_{i+1} \\ ... & ... & ... & ... \\ \mathbf{R}_i & \mathbf{R}_{i+1} & ... & \mathbf{R}_{2i+1} \end{bmatrix} \tag{19}$$

Here, 2i corresponds with the largest number of time lags. The correlation matrices are defined as:

$$\mathbf{R}_k = E(\{y_{n+k}\}\{y_n\}^T) \tag{20}$$

where the vector $\{y_n\}$ is the monitored quantities (here acceleration) from all channels, for sample n. The sample-shift k gives the time lag, as time lag is defined as:

$$\Delta t = k * f_s^{-1} \tag{21}$$

where Δt is the time lag and f_s is the sampling frequency.

The decomposing of the block-Handel matrix corresponds to the observability and controllability matrices. The decomposition is as follows:

$$\mathbf{H}_i = \mathbf{O}_i \mathbf{\Gamma}_i \tag{22}$$

where the observability matrix is defined as follows:

$$\mathbf{O}_i = \begin{bmatrix} \mathbf{C} \\ \mathbf{CA} \\ \mathbf{CA}^2 \\ ... \\ \mathbf{CA}^{i-1} \end{bmatrix} \tag{23}$$

and the controllability matrix is defined as follows:

$$\mathbf{\Gamma}_i = [\mathbf{G}, \mathbf{AG}, ..., \mathbf{A}^{i-1}\mathbf{G}] \tag{24}$$

where the matrices A and C are the discrete state matrix and the discrete output matrix, respectively, from the stochastic state space model describing the problem:

$$\{z_{n+1}\} = \mathbf{A}\{z_n\} + \{w_n\} \tag{25}$$

$$\{y_n\} = \mathbf{C}\{z_n\} + \{v_n\} \tag{26}$$

where $\{z_n\}$ is the state vector, $\{y_n\}$ is the output vector, $\{w_n\}$ is the process noise, and $\{v_n\}$ is the measurement noise. The matrix $\mathbf{G}$ is defined as:

$$\mathbf{G} = E(\{z_{n+1}\}\{y_n\}^T) \tag{27}$$

After pre-multiplying the block-Handel matrix with $\mathbf{W}1$ and post-multiplying with $\mathbf{W}2\mathrm{T}$, it can be decomposed using singular value decomposition (SVD), and then truncated as follows:

$$\mathbf{W}_1\mathbf{H}_i\mathbf{W}_2^T = \begin{bmatrix}\mathbf{U}_1 & \mathbf{U}_2\end{bmatrix}\begin{bmatrix}\mathbf{\Sigma}_1 & \mathbf{0} \\ \mathbf{0} & \mathbf{\Sigma}_2\end{bmatrix}\begin{bmatrix}\mathbf{V}_1^T \\ \mathbf{V}_2^T\end{bmatrix} \tag{28}$$

$$\approx \begin{bmatrix}\mathbf{U}_1 & \mathbf{U}_2\end{bmatrix}\begin{bmatrix}\mathbf{\Sigma}_1 & \mathbf{0} \\ \mathbf{0} & \mathbf{0}\end{bmatrix}\begin{bmatrix}\mathbf{V}_1^T \\ \mathbf{V}_2^T\end{bmatrix} \tag{29}$$

$$= \mathbf{U}_1\Sigma_i\mathbf{V}_2^T \tag{30}$$

The truncation executed here is an approximation due to noise in the system. In practice, Σ will be non-zero values, and the order has to be specified manually. The optimal order is not known a priori, thus a stabilization plot is used to distinguish between physical and spurious poles, using multiple orders.

By combining the equations 22 and 28 an estimation of the observability matrix can be established as follows:

$$\mathbf{O}_i = \mathbf{W}_1^{-1}\mathbf{U}_1\mathbf{\Sigma}_1^{1/2} \tag{31}$$

The state matrix can then be computed as follows:

$$\mathbf{A} = \mathbf{O}_{down_n}^{+}\mathbf{O}_{up} \tag{32}$$

where the two matrices denoted down and up both are subsets from the observability matrix, but without the first and last l rows, respectively. + denotes the pseudo-inverse of the matrix. The output matrix $\mathbf{C}$ establishes the physical mode shapes and is retrieved from the first l rows of the observability matrix:

$$\mathbf{C} = \mathbf{O}_{i1:l} \tag{33}$$

The discrete eigenvalues and the system eigenvectors can be established by performing an eigenvalue decomposition. These can then be transformed into the continuous eigenvalue and eigenvectors with coordinates referring to the sensor coordinates as follows:

$$\lambda_r = ln(\hat{\lambda}_r) * f_s^{-1} \tag{34}$$

$$\Phi = \mathbf{C}\Psi \tag{35}$$

where the modal transformation matrix is defined in equation 35, has columns that refer to the identified mode shapes $\{\psi\}_r$. Here r is the mode index.

2.8 Modal Assurance Criterion (MAC)

The modal assurance criterion is a function that provides a measure of consistency between modal vectors, or estimates of modal vectors[6]. It can provide a method for easily comparing estimates of modal vectors originating from different sources and provide an additional factor of confidence in the evaluation of a modal vector from different excitation locations or different modal parameter estimation algorithms. Two comment sources of modal vectors to compare are modal vectors from an FE analysis and experimentally determined modal vectors. By this method, modes van be compared and contrasted, such that corresponding modes are paired and all others are discarded.

The MAC is defined as a scalar constant relating the degree of consistency (linearity) between one modal and another reference modal vector as follows:

$$MAC_{cdr} = \frac{|\{\psi_{cr}\}^T\{\psi_{dr}^*\}|^2}{\{\psi_{cr}\}^T\{\psi_{cr}^*\}\{\psi_{dr}\}^T\{\psi_{dr}^*\}} \tag{36}$$

Here, ψ refers to the modal coefficient, c, and d refers to the degree of freedom, r refers to the mode, and * denotes the complex conjugate.

MAC takes on a value ranging from zero to unity (0 to 1), where zero represents no consistent correspondence, and unity represents consistent correspondence. Note that MAC is standardized by the magnitude of the vectors, resulting in values that range from zero to unity.

MAC can only be used for indicating consistency, not orthogonality or validity. If errors are consistent across methods and sources the MAC number may be near unity, but the error is not validated. The underlying assumptions may cause consistent errors for all model vectors for several test conditions. Assumptions should be carefully considered.

2.9 Updating of FE-Model

The initial FE-model created for a system is rarely in complete agreement (MAC is unity and frequencies are identical) with the system identification results. To increase the model's accuracy in predicting the system, it can be updated.

In order to perform model updating, experimental data is required. Since the FE model and system identification are not in complete agreement, it is required to pair modes together[7]. For pairing, MAC numbers and natural frequencies can for instance be used.

The purpose of model updating is to predict system behavior exposed to different loading arrangements, or different structural configurations. As the updated model aims for predictive use, any increase in agreement must be achieved through rectifying inaccuracies in modeling assumptions rather than implementing other modifications that might not be physically meaningful[8].

When executing model updating, imperfections in the modal analysis should be taken into consideration.

2.10 Structural Health Monitoring (SHM)

Structural Health Monitoring is defined as the process of implementing an automated and online strategy for damage detection in structures[9]. SHM can provide increased life-safety benefits by continuous monitoring, and economic benefits by improved inspection efficiency and minimized unplanned downtime. For bridges, there are several approaches for applying SHM. For this project, the focus will be on the model-based approach. In the model-based approach, a finite element model (FE model) is established, according to the drawings and material data. This FE model is updated based on the system identification of the bridge. By analyzing damages introduced to the updated model, the model, combined with continuous measurements and system identification, can reveal the existence and location of damages.

For this project, the method of model-based approach of SHM is performed, but not automated or online, and is thus not SHM. This limited version of SHM is referred to as structural monitoring.

3 FE-model

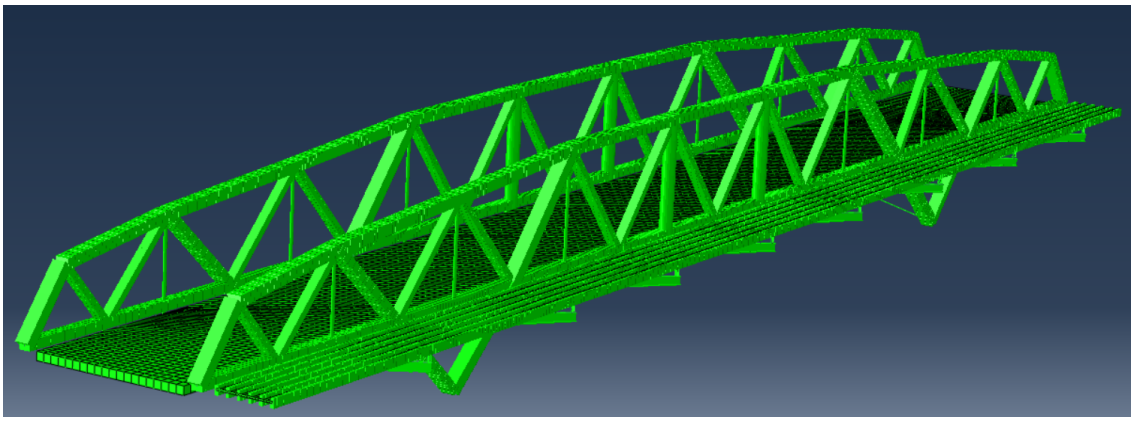

Figure 2: Finite Element model of Hell Bridge

The Finite Element model of Norsenga Bridge, shown in Figure 2, was modeled in ABAQUS, specifically ABAQUS keyword for this project. A significant amount of time was spent on developing the method for generating the model, as well as the modeling itself. How the model was generated and the parameters of the model are described under.

3.1 Nodes and Elements

The model is created using nodes with defined coordinates, and creating elements between them.

The size of the elements is important as they decide the accuracy of the solution and the run time. In order to make the element size flexible, a method for automatically defining nodes and elements has been created. Key nodes, such as the joints of the trusses, have been manually defined by x, y, and z coordinates in an Excel sheet. Elements between nodes are then defined in a separate Excel sheet, with additional information such as the section type, dimensions, and material. There is a separate Excel sheet for the different element types; beam elements and shell elements. This Excel file is then read by a developed Python script, that reads the nodes and the elements, then interpolates them and creates new nodes and elements. The elements are interpolated to have a maximum desired length and a minimum of the desired number of divisions. These new nodes and elements, along with the old nodes, are printed into an .inp file. Elsets and sections are also printed into the .inp file. Thus changes in the Excel file, or changes for the element length can quickly be generated into an .inp file that can be read by ABAQUS. A drawback of the chosen method is that the model created by the .inp file cannot be edited in ABAQU'S user interface.

Information on the chosen element and the number of elements for each element type is displayed in Table 1. B31 is chosen for beam elements since it is computationally cheap and has good general characteristics. Similarly, S4R is chosen for the shell elements. The maximum length of beam elements is 0.25 meters and the minimum

Table 1: Information on the FE model

Element type	Element	Number of elements	Maximum element length	Minimum element divisions
Beam Element	B31	6807	0.25 m	4
Shell Element	S4R	7600	1.00 m	21

amount of divisions is 4. This is because some of the elements defined in the Excel sheet are short, and thus have no need for many divisions. For longer elements, 0.25 meters per element gives a high enough resolution, because of the great size of the bridge. For the shell elements, the maximum length of elements is 1 meter and the minimum amount of divisions is 21. In practice for the model defined in Excel, all elements are divided into 20 by 20 elements.

The hangars connecting the trusses to the main beam are all pipes, except for the four large hangers in the middle. They are built as octagonal cross-sections. However, also these are modeled as pipes since a pipe is very close in function.

For the main beams supporting the bridge decks, there is tapering. That is a continuous change of the cross-section along the beam. In order to model this, several nodes and elements have been manually defined and given a cross-section that matches the tapered beam at that point. The accuracy of this solution has been assumed to be acceptable since the beam retains the intended mass and stiffness.

3.2 Connections

All connections are fixed, that is, no rotation between the two connected elements is allowed, and the connection remains completely stiff. In reality, all connections will be something between fixed and hinged. This is likely the largest contributor to inaccuracies in the model. This is done due to difficulties with modeling springs and hinges in ABAQUS keyword. Having all connections fixed makes the model too stiff, and will increase the natural numerical frequencies. The hangers and cross-bracings are likely to have connections almost perfectly hinged. In the numerical model, they might resemble the actual behavior, since the cross sections are so small that they do not transfer much moment anyway. The joints of the trusses however might have greater impacts on the dynamic response, which hinders the model's ability to predict the dynamic behavior of Norsenga Bridge.

It is worth noting the connection between the main bridge deck and its supporting beams. In reality, they are only loosely connected, mainly through the friction between them. They can to some degree displace independently from each other. In order to simulate this behavior with completely locked connections, the bridge deck is only connected to the beams at its edges. The beams are not loaded on the middle and are thus not subjected to large bending forces. This is expected to have a low impact on the global dynamic results of the model since no mass or stiffness is lost from this modeling choice.

3.3 Material

Three materials are defined for the bridge. One for the structural steel used on the bridge, and two different classes of structural timber.

The parameters of the materials defined are given in Table 2

Table 2: Information on the FE model

Material	Stiffness [MPa]	Density [kg/m3]	Poisson ratio	Type
s355	210 000	7850	0.3	Isotropic
GL32h	13.5	440	0.3	Isotropic
GL30h	13	430	0.3	Isotropic

Both GL32h and GL30h are defined as isotropic. This is technically not correct as structural timber is not isotropic, but since the timber is mostly loaded in the strong axis, this is assumed to be an acceptable simplification with negligible effects on the results. The poison ratio is set to 0.3, but will not have an impact on the dynamic behavior of the material.

3.4 Additional Mass

As previously stated in Equation 6, the mass of the structure is important for global dynamic behavior, as it decreases the natural frequencies. Norsenga Bridge consists not only of structural parts but also dead load in the form of asphalt and safety rails. To account for this, an additional mass has been modeled as point masses. Both the asphalt and safety rails are modeled as point masses distributed over the whole bridge deck. This applies to the main bridge deck and the pedestrian bridge deck. This is done by assigning a distributed mass to the shell elements defined in the Excel sheet described in Section 3.1. The area of the shell element is then calculated, and the total additional mass is distributed evenly on all the nodes in the element.

Modeling the safety rails as distributed mass over the bridge deck is technically wrong since all the mass is put on the edges. However, for the purpose of dynamic analysis, such a simplification is considered acceptable.

The true weight of the asphalt is not known but is estimated. This is also true for the safety rails. The total additional mass per m2 is given for the main bridge deck and the pedestrian bridge deck in Table 3. As the additional mass makes up 38% of the total mass, this is important to the dynamic response of the structure, especially the natural frequencies.

The total additional mass is 270 412 kg, making the total mass of the system 712 850.9 kg.

Table 3: Additional Mass

-	Main Bridge Deck	Pedestrian Bridge Deck
Thickness of cast asphalt [mm]	30	0
Density of cast asphalt [kg/m3]	1500	1500
Thickness of asphalt [mm]	97.5	40
Density of asphalt [kg/m3]	2000	2000
Thickness of TOPEKA [mm]	12	10
Density of TOPEKA [kg/m3]	2916.67	2916.67
Line weight of safety rails [kg/m]	45	25
Half width of bridge deck [mm]	42500	1750
Additional mass [kg/m2]	286	123
Total additional mass [kg]	229 730	40 682

3.5 Boundary Conditions

Boundary conditions are used at nodes assumed to be restrained from motion. These are at the bottom of the support, the ends of each truss, and the ends of the bridge deck. The nodes are restrained from displacements in the vertical direction and either the along bridge direction or across bridge direction. None of the nodes are restrained from rotation.

Using these boundary conditions on the bottom supports and the truss end is very close to reality, as it is connected to the top of large concrete supports. However, the boundary conditions at the bridge deck ends are more ambiguous. Only two nodes at each deck end are restrained from motion in the y and z direction. This is done to replicate the continuous transition between the bridge deck and the road.

Restraining displacement at these points increases the stiffness of the model. Through testing, it was found that the first mode shape does not happen if the bridge deck is restrained in the along-the-bridge direction.

3.6 Finite Element Results

The results from the FE-model give the first 200 natural frequencies and their corresponding mode shapes.

It is important to distinguish between local and global modes. Global modes activate large parts, or the entire structure, while local modes only activate a small part of the structure, for example, one beam section. Only the global modes are relevant to the response. Local and global modes can be distinguished visually in the visualization in ABAQUS, or by evaluating the modal participation factor. A high modal participation factor indicates a global mode.

For this model, many local modes were discovered for the pedestrian bridge, since it has slender beams and a thin deck. The cross- bracings beneath the bridge also have a lot of local modes. An example of a local mode is found in Figure 3.

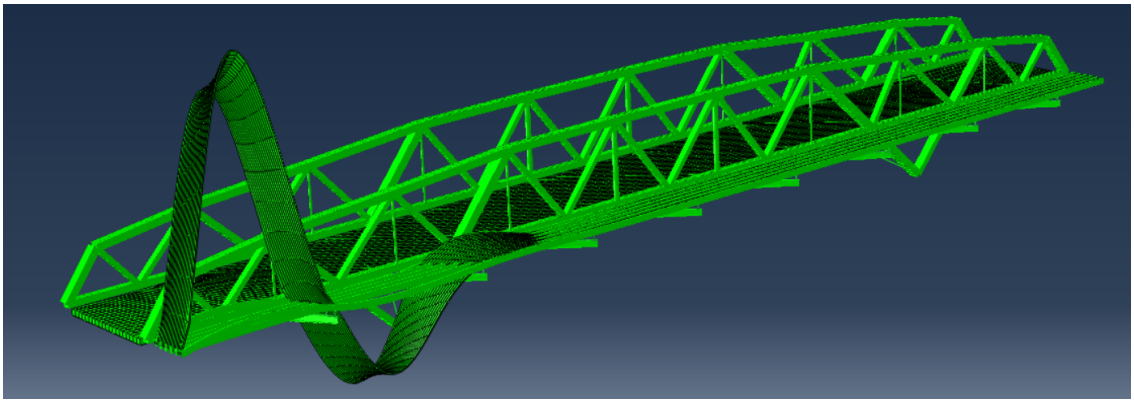

Figure 3: Example of a local mode of the pedestrian bridge deck.

The lower frequency modes generally have higher modal masses and dominate the response of the structure. Therefore we only consider the lower natural frequencies. The first 14 frequencies up to 4 Hz, which are evaluated as global modes, are given in Table 4. The first horizontal mode (mode 3 in the analysis) and the first vertical mode (mode 29 in the analysis) are displayed as examples in Figure 4 and 5, respectively. Note that the vertical mode has large deformations of the pedestrian bridge deck.

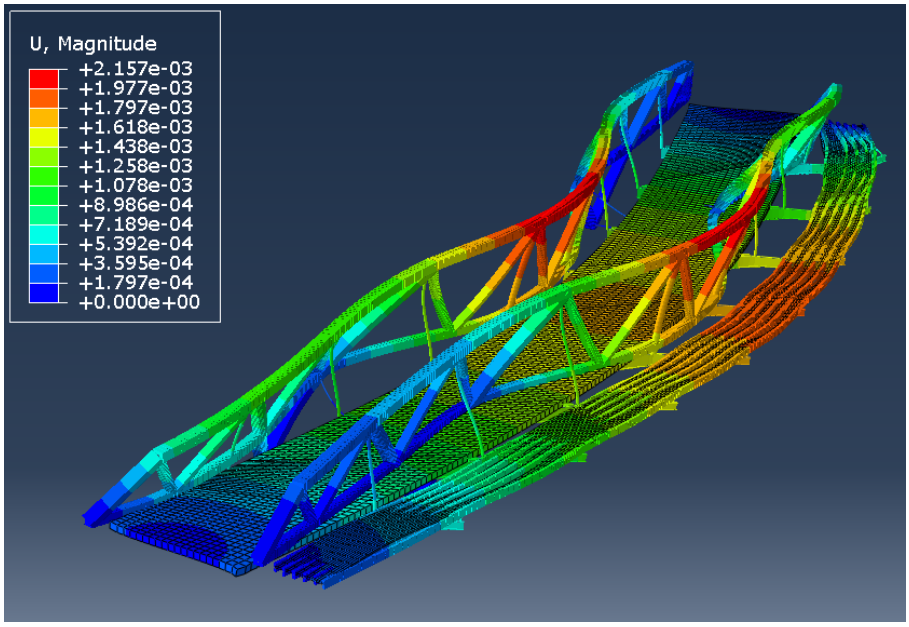

Figure 4: First global mode from the FE-model, the first horizontal mode.

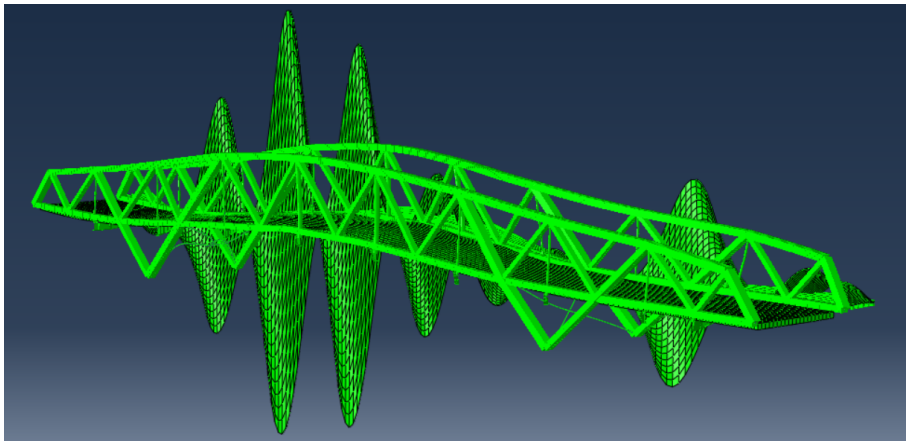

Figure 5: First vertical mode from the FE-model.

Table 4: Natural frequencies from FE-model up to 4 Hz

Mode number	Gobal Mode Number	Frequency [Hz] from FE-model	Mode
3	1	1.4077	First Transversal Mode
5	2	1.8322	Southwest Mode
6	3	1.9024	Northeast Mode
8	4	2.1427	Northwest Mode
9	5	2.2357	Southeast Mode
10	6	2.5505	Odd Third Transversal Mode
14	7	2.7325	Third Transversal Mode
15	8	2.8146	Third Transversal Mode
17	9	3.0163	North Focused Third Wall Mode
18	10	3.0859	Third Wall Mode
23	11	3.3818	Third Transversal Mode Stiff Middle
29	12	3.7854	First Vertical
32	13	3.9628	Fourth Transversal Mode
33	14	3.9860	Fourth Wall Mode

Modes 2, 3, 4, and 5 are modes mainly involving one corner of one truss. Each mode is one of the corners. These are special modes that will be used later in Section 7. The fifth mode, the southeast mode is displayed as an example in Figure 6.

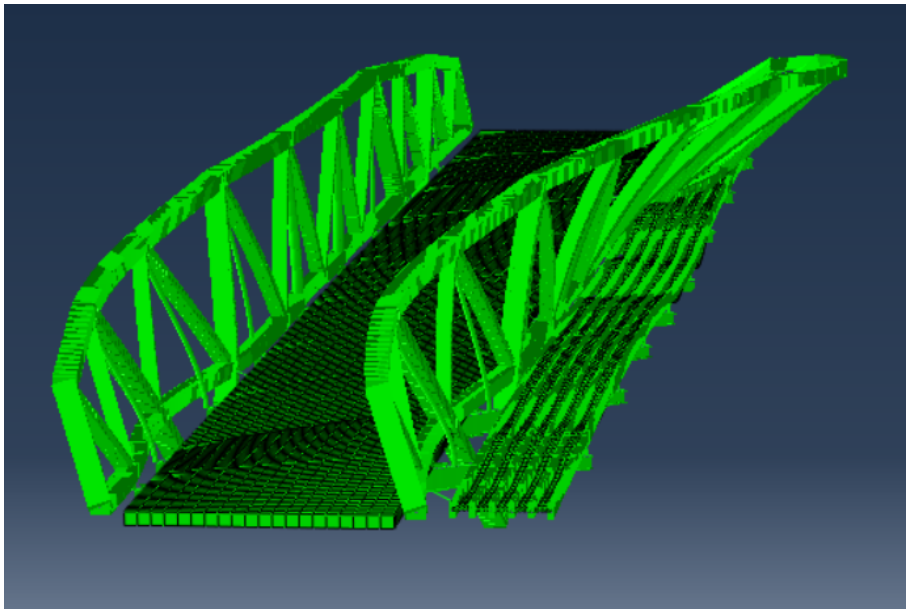

Figure 6: The southeast mode.

For the 15 modes defined in Table 4, the deformation at the location of the accelerometers on Norsenga bridge, is extracted. These are used, along with the natural frequencies, to determine the accuracy of the FE model. The nodes representing the location of the accelerometers are highlighted in Figure 7. Note that all accelerometers are on the trusses. Thus only the shape of the trusses will be compared to modal analysis of the measurement data.

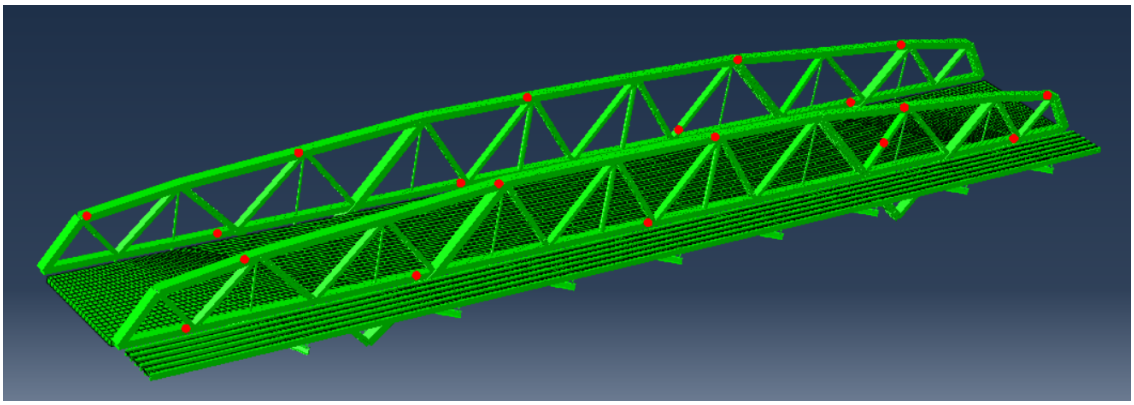

Figure 7: Location of accelerometers highlighted on the FEM model.

4 Instrumentation

Norsenga Bridge was instrumented on the 9th and 10th of October in 2023. Due to the safety hazards of working over an active railway, with high voltage, the instrumentation was planned for a weekend when the railway was shut down nationwide for maintenance. This chapter will describe in detail the relevant instrumentation.

4.1 Accelerometer

Figure 8: One of the accelerometers installed on the bridge.

For the analysis, acceleration measurement is needed. For the purpose of measuring accelerations at Norsenga Bridge, accelerometers produced by DEWESoft have been used. The IOLITE 3xMEMS-ACC can measure vibrations in 3 directions. It has a 25 $\mu g/\sqrt{Hz}$ spectral noise density, and has a shock rating of 50g[10]. It is waterproof and is built to handle temperatures between -20 °C and 60 °C, and should therefore withstand the environment at the bridge site. An image of one of the accelerometers installed on the bridge is found in Figure 8.

4.2 Set Up Scheme

The bridge has been equipped with several measuring devices. The bridge has accelerometers, strain gauges, wind measurements, and thermostats, all feeding their measurements in real-time to a DEWESoft computer recording it all. In this analysis, only the accelerometers are used. However, the wind speed and temperature are checked for the recording used for the analysis.

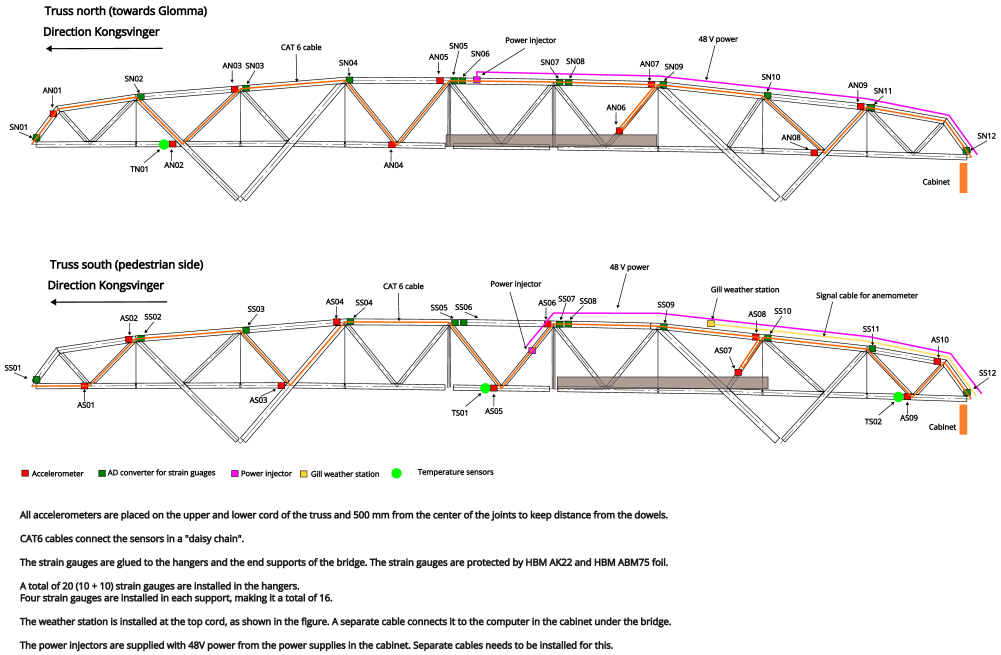

Figure 9: The set up scheme for Norsenga Bridge.

There are in total 19 accelerometers instrumented on the bridge. 10 are located on the south truss, and 9 are located on the north truss. They are placed so that there are no "overlapping" junctions. That is, if one junction has an accelerometer on the south truss, there is no accelerometer on the north truss for that junction. This is clear in Figure 9, which displayed the setup scheme. This scheme was chosen in order to capture a high number of low-order mode shapes of the bridge while not using more accelerometers than necessary. Both sides are measured in order to have an accurate representation of the mode shapes and are especially helpful in distinguishing the wall modes and the transverse modes. This configuration has been employed in numerous bridge constructions by the institute previously, demonstrating a track record of high performance.

4.3 Practical Installation

In the setup scheme, the accelerometers are placed at the center of the junctions. However, since the junctions have bolts in the center, the accelerometers are placed at some horizontal distance from the center. They are either placed 0.5 meters, 1 meter, or 1.5 meters from the center, depending on how far the junction is bolted. These distances are chosen so that which distance used is visible, to the naked eye. An example is given in Figure 10. For this junction, the accelerometer is 0.5 meters from the center of the junction.

Figure 10: Example of the distance between the center of the junction to the location of the accelerometer.

4.4 Data Quality

The accelerations are measured with a sampling frequency of 100 Hz.From the FE analysis, we can see that we are most interested in frequencies up to 4 Hz, and our sampling frequency is thus adequate. The general quality of the data seems to be good, as there are no accelerometers that clearly give false data.

5 System Identification

The system identification of Norsenga Bridge was performed using 2 methods; FDD and SSI. Using a 20-minute segment of a recording of 10 accelerometers on the south truss and 9 accelerometers on the north truss, natural frequencies and corresponding mode shapes have been identified.

5.1 Method

Two methods are chosen for the system identification; FDD and SSI. Both of these methods are proficient at identifying natural frequencies and corresponding mode shapes, but both methods require some engineering insight to determine relevant modes and frequencies, as there are some detected that are false. The results from the two methods are compared to each other in order to verify each other.

5.1.1 FDD

The basic theory behind FDD is described in Section 2.6. The procedure for the practical implementation of FDD is described here.

Before using the recorded data, it is important to detrend the data. This is in order to ensure that recordings fluctuate around zero and that the fluctuation point does not change over time. A low-pass filter is applied to filter out data far above the range of interest. For filtering, the Butterworth filter is chosen. The filter order chosen is 3, and the cutoff frequency is 48.

The cross-spectral density of the recording is calculated using Welch's method. Welch's method divides the recording into several windows and uses an average of all the cross-spectral densities from each window. It is important to choose an appropriate number of windows, such that the averaging is somewhat smooth, but retains high resolution. From the FE model, we have the lowest expected natural frequency of about 1.4 Hz, the minimum time window should be able to contain more than two periods. Here, that is about 1.4 seconds. The chosen length of the window is 100 seconds and is more than long enough to identify the first natural frequency. This length is chosen in order for the two last digits of the identified frequencies to not be rounded off. For Welch's method, some overlap between the windows can be chosen, in order to effectively increase the sample size. However, the sample size chosen is 1200 seconds (20 minutes) long. 12 windows are enough, and thus no overlap is chosen.

Singular value decomposition is performed on the cross-spectral density matrix for each frequency. This gives the mode shape and singular values for that particular frequency. Note that the calculated mode shape from the SVD is only real if the frequency is a natural frequency.

In order to find the natural frequencies, peak-picking is performed on the first singular value. A peak in one of the singular values indicates a natural frequency. Since the first singular value has the highest impact, peak-picking is only performed on the first singular value. The peak-picking function from Scipy is not perfect. By

evaluating the peaks of the singular value spectrum, falsely detected peaks may be determined. Also by evaluating the mode shapes visually, and using engineering insight to ensure that the shape is somewhat realistic. Peaks not detected are also manually added. The three first singular values are plotted over the frequency in Figure 11 for frequencies up to 4 Hz. The red dots indicate a natural frequency. The unrealistic peaks have been removed.

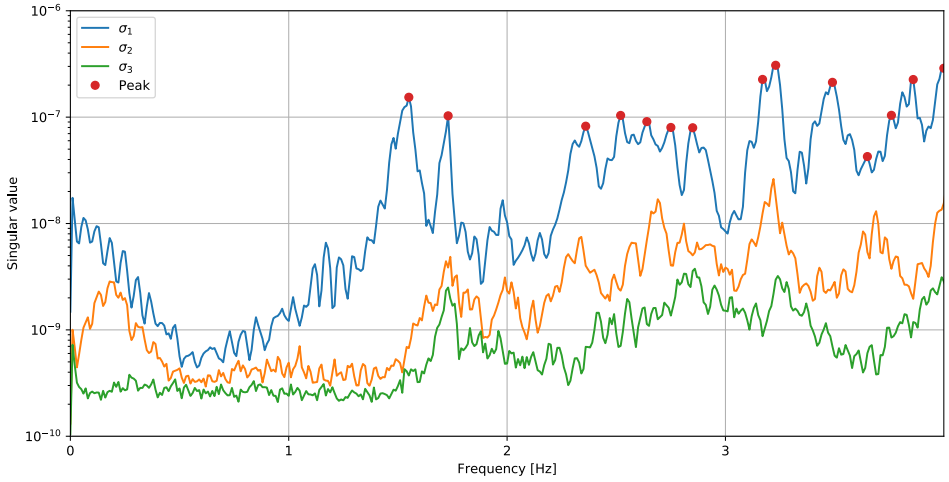

Figure 11: Singular value spectrum from FDD.

The mode shapes are then visualized in 2D plots. An example of the visualization is given in Figure 12.

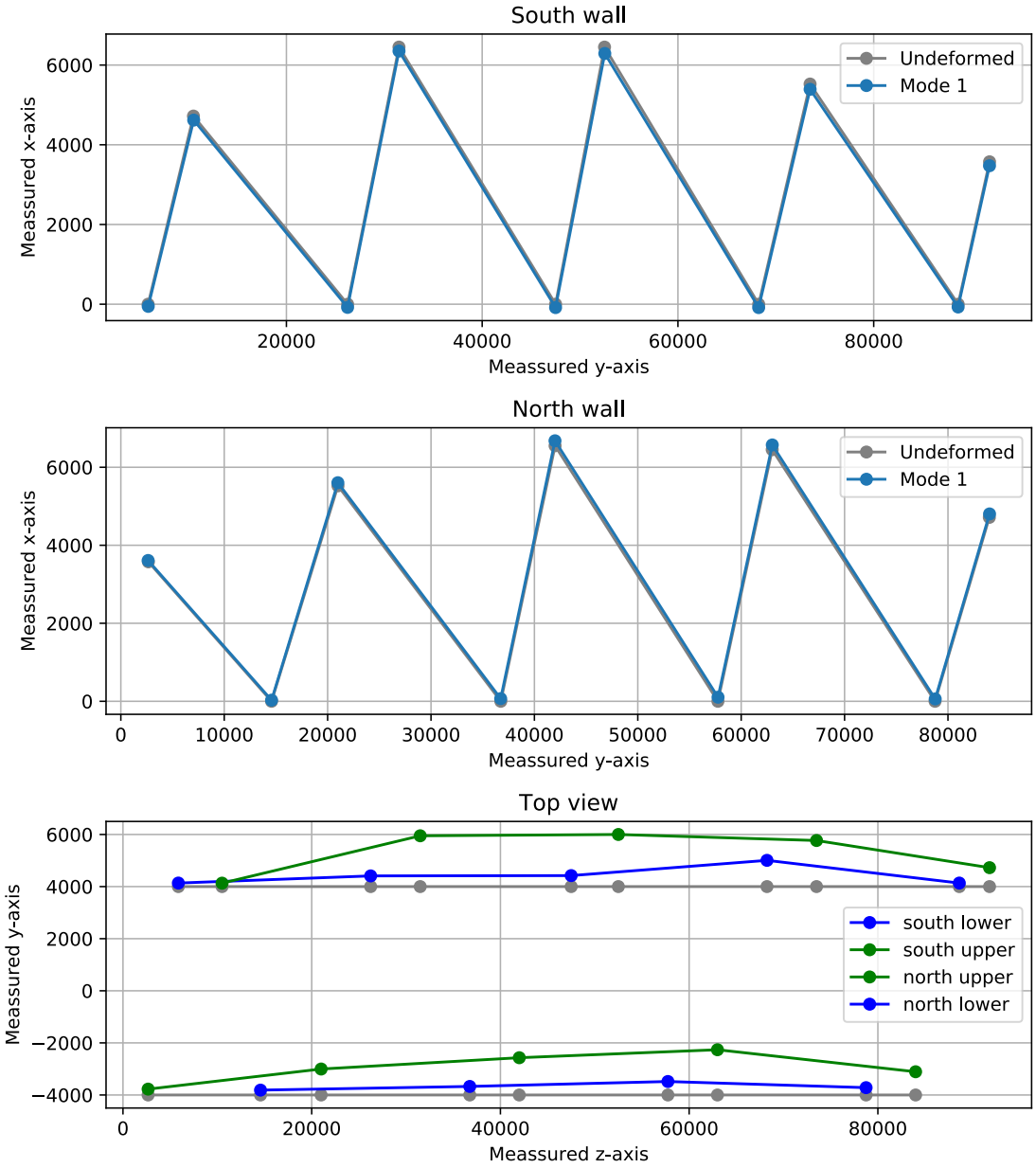

Figure 12: Visualisation of Mode Shape from FDD.

After the procedure, natural frequencies and corresponding mode shapes are identified.

5.1.2 SSI

The theory behind SSI is described in Section 2.7. The settings applied in the SSI are described here.

Before using the recorded data, the data is again detrended identically to the FDD. For the practical implementation of SSI, tools from the Python package koma.oma[11] were used.

Before performing the cov-SSI, it is necessary to define two input parameters impacting the results. The first parameter to define is the time shift. In order to have a successful system identification, it is necessary that the time shift is long enough to capture the signal until it is damped out. A long time shift is very computationally expensive as the workload increases exponentially with the time shift. Therefore the time shift is chosen to be as short as possible. For Norsenga bridge it is set to 2 seconds. When the SSI results are compared to the FDD results, 2 seconds seems reasonable.

The other parameter is the number of orders. The SSI creates poles for every other order and is theoretically more accurate for higher orders. The chosen number of orders is 160.

No stability criteria are applied before plotting the poles. The poles detected from the 13th of November 2023 are displayed in Figure 13. The grey lines in the background are the frequencies detected in the FDD. Note that for the high orders. The frequencies between the two modes are very close. The mode detected at a very low frequency, about 0.1 Hz, is assumed to be falsely detected and is discarded from further analysis.

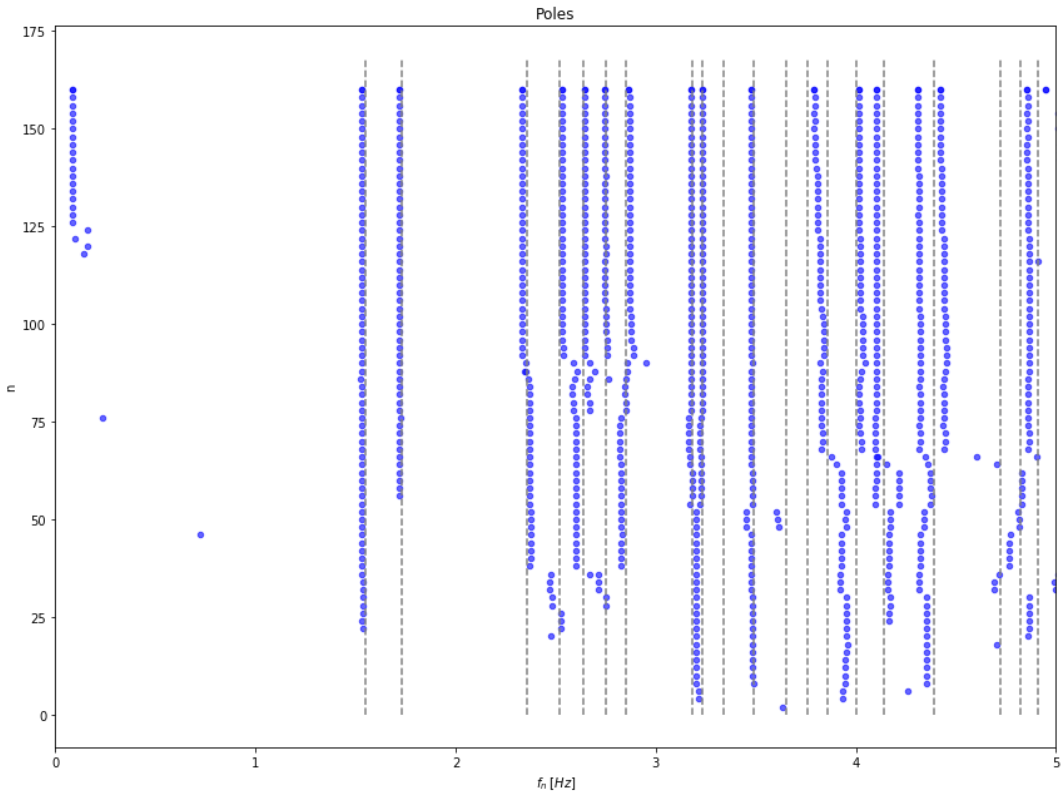

Figure 13: Stability plot of the SSI with grey lines as the peaks from the FDD.

After the procedure, natural frequencies and corresponding mode shapes are identified. The mode shapes are visualised similarly to the FDD as shown in Figure 12.

5.2 Measurment Data

For the system identification, a recording of Norsenga Bridge on the 13th of November 2023 between 18.43 and 00.00 (midnight) was provided. The recording was from the 19 accelerometers on the north and south truss. The sampling frequency is 100 Hz.

The main dynamic loads of the bridge are from traffic and wind. Thus the traffic situation along with the wind conditions during the recording is important for system identification. Noresnga Bridge is only open to traffic in one direction at a time, and only one truck at a time, due to potential issues with the structure detected after the collapse of Tretten Bridge in 2022. This is enforced by traffic lights at each end of the bridge. The consequence is that for any chosen segment of the recording, there will regularly be no traffic load. For our recording traffic is regular. The traffic can be observed in the acceleration recordings such as in Figure 14. It is important to not maintain a constant traffic load since the weight of heavy trucks can alter the system behavior by adding mass. From the wind measurements, we can see that the wind speed was mostly about 3 m/s, and up to 6 m/s for short moments. The temperature was -4.5 °C.

For system identification, white noise is assumed, such that the response of the structure is due to the dynamic behavior of the structure and not the load. On-and-off traffic in combination with wind is assumed to be broad-banded and should reveal the system's behavior. However, there is some variation between every recording, and some recording-specific response is expected.

An example of the recording from one accelerometer in all 3 directions is given in Figure 14. Traffic is visible as acceleration spikes. Each plot is scaled independently.

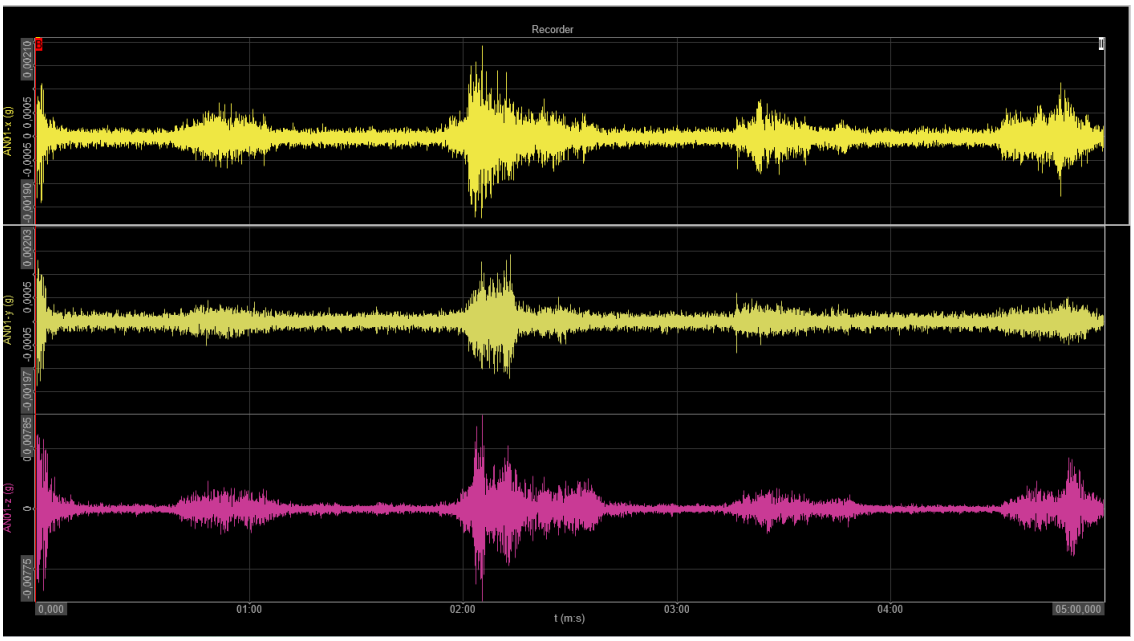

Figure 14: 5-minute recording of accelerometer AN01 in x, y, and z direction in descending order.

5.3 System Identification Results

The results from the system identification are the natural frequencies and their corresponding mode shapes from the FDD and SSI. Some of these are expected to be falsely detected or duplicates of each other, even after excluding the obvious false frequencies and mode shapes. In order to evaluate the quality of the two methods, we can compare the mode shapes detected at the same frequency for both methods. To compare the mode shapes, we use MAC. The results of the comparison are given in Table 5. Frequency error is defined as:

$$FE = \frac{f_1 - f_2}{f_1} \tag{37}$$

Table 5: Matching natural frequencies and mode shapes from FDD and SSI

SSI Mode	FDD Mode	SSI Natural Frequency	FDD Natural Frequency	Frequency Error	MAC Number
1	1	1.53	1.55	1.3%	0.9961
2	2	1.72	1.73	0.6%	0.9843
3	3	2.33	2.36	1.3%	0.8534
4	4	2.53	2.52	0.4%	0.9087
5	5	2.65	2.64	0.4%	0.9046
6	6	2.75	2.75	0.0%	0.9262
7	7	2.87	2.85	0.7%	0.9633
8	8	3.18	3.18	0.0%	0.8708
9	9	3.23	3.23	0.0%	0.9082
10	10	3.48	3.49	0.3%	0.9806

Table 5 compares the first 10 true modes from SSI and FDD with the approximately same frequencies. Frequency errors and MAC numbers are used to determine the pairing quality. All paired modes are of high quality. Since both methods detect the same mode shapes from the recording, we can assume they are all real and accurately represent the dynamic behavior of the bridge. The methods applied and their results are validated by each other. These 10 modes will further be used to evaluate the accuracy of the finite element model.

An example of two paired modes from the FDD and SSI is provided in Figure 15. In this 2D plot, the mode shapes of the 10th mode from both methods are plotted together.

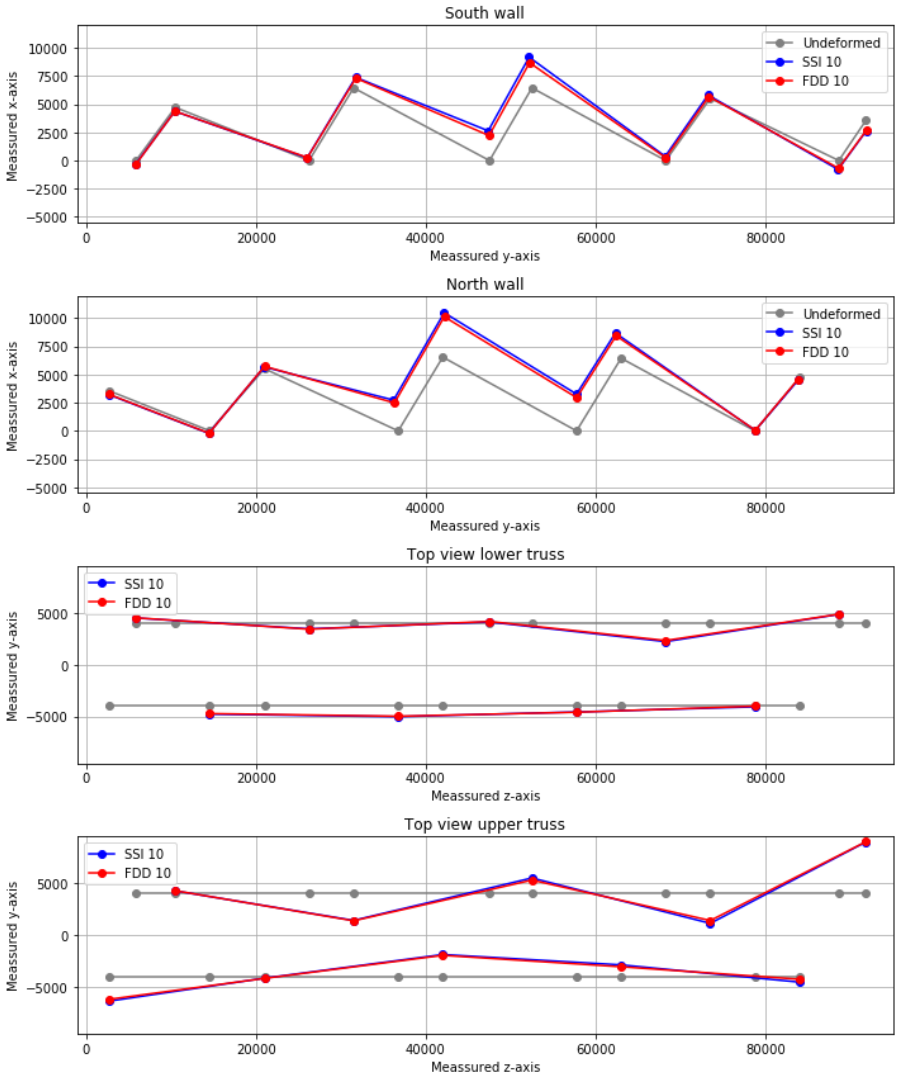

Figure 15: Comparison between mode shape 10, the 1st vertical mode, from SSI and FDD.

The two upper subplots in Figure 15 show the displacement of the measurement points from the side. The uppermost subplot is of the south truss and the one below is of the north truss. The two lower subplots are from a top view, showing sideways displacement. The lower subplot is only of the measurement points located at the top of the trusses, and the one above is only of the measurement points located at the bottom of the trusses The natural frequency for the mode is 3.48 Hz for both methods and the MAC number is 0.98. This is a near-perfect agreement between the two methods.

Note from Figure 15, displacements of the upper truss are greater than displacement for the lower truss. Even for this vertical mode, sideways displacement of the upper truss is great. For most modes, the mode shapes are dominated by sideways displacements in the upper truss.

5.4 System Identification of Alternative Recording

In order to verify that the system behavior has been identified and that the loading case was broad-banded, system identification was performed on another recording of the bridge.

This recording is from the 11th of December 2023 at 14.40 in the afternoon. The temperature during the recording was about -1.5°C, and the wind speed was about 4 m/s. From the spikes in the accelerometers, there seems to be regular traffic. These conditions are very similar to our main recording of the 13th of November.

Comparing the SSI of the two recordings, the frequencies, and the corresponding mode shapes from the two recordings are compared.

The stability plot of from the SSI of he alternative recording is given in Figure 16. The grey dotted lines in the background are the results from the SSI of the main recording. From the figure we can see that the identified frequencies from the two recordings are very similar for most frequencies. Noteworthy frequencies with more distance than the others are the 5th frequency from the main recording (about 2.7 Hz) as well as the two frequencies between 3 and 3.5 Hz. For these, the frequency is lower for the alternative recording. Also note that there are more unstable poles at high orders than there were for the main recording, displayed in Figure 13. Some recording-dependent variation is expected for the system identification. Figure 16 displays no major differences between the frequency results of the two recordings. All the same stable poles are detected from both recordings for the frequency range relevant to this project.

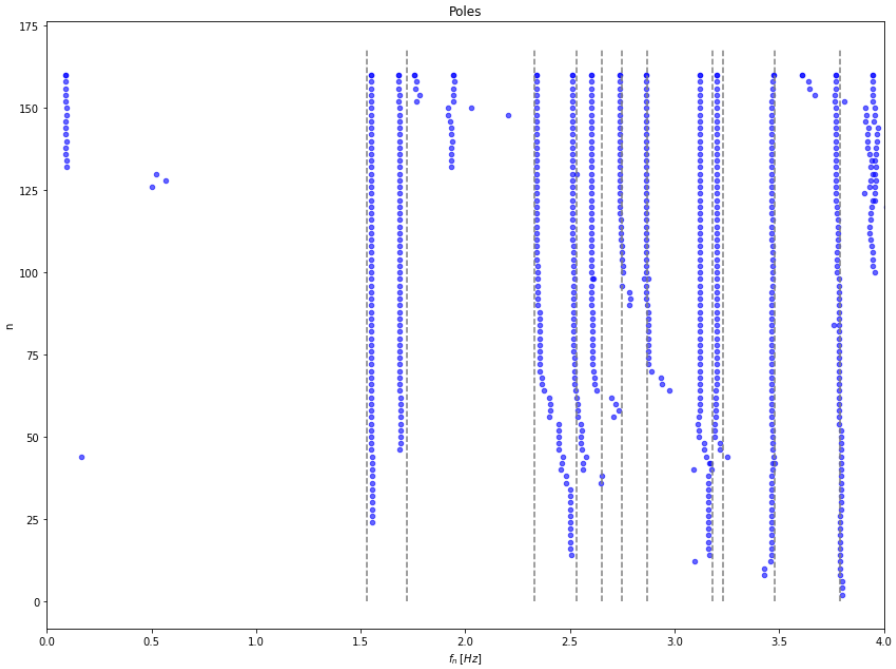

Figure 16: Comparison between SSI of alternative and main recording.

The comparison between the stable poles from the main and the alternative record-

ing is given in Table 6. Note that most MAC numbers (9 out of 11) are higher than 0.8. Mode 3 and 5 have lower-quality agreements. The Frequency error is also small for all modes, but noticeable for the 3 frequencies discussed above. The results from the two recordings are similar, but less so than those of the results from the FDD and SSI for the main recording given in Table 5.

Table 6: MAC and frequency comparison of alternative and main recording

SSI Main Mode	SSI Alt Mode	SSI Main Natural Frequency	SSI Alt Natural Frequency	Frequency Error	MAC Number
1	1	1.53	1.55	1.3%	0.9424
2	2	1.72	1.68	2.3%	0.8915
3	3	2.33	2.34	0.4%	0.7125
4	4	2.53	2.51	0.8%	0.8970
5	5	2.65	2.60	1.9%	0.6476
6	6	2.75	2.74	0.4%	0.8509
7	7	2.87	2.86	0.3%	0.8105
8	8	3.18	3.12	1.9%	0.9681
9	9	3.23	3.20	0.9%	0.8928
10	10	3.48	3.47	0.3%	0.9488
11	11	3.79	3.77	0.5%	0.8666

The results from the SSI of the alternative recording are similar to the results from the SSI of the main recording. From this, we can conclude that it is the system behavior that has been identified, and not the loading case. The dynamic load must therefore be sufficiently broad-banded for system identification. The results from the alternative recording will not be further used in the report, only the results from the main recording.

5.5 System Identification and Finite Element Comparison

Here the results from the system identification and finite element analysis will be compared. Only the SSI and FEM results will be compared, as the similarity between SSI and FDD has been verified in Table 5. Similarly to the comparison between the SSI and FDD, frequency errors and MAC numbers describe how similar they are. All global modes from the FE-analysis up to 4 Hz and 10 first modes from the SSI, up to 3.5 Hz, are included in the comparison. The goal is to pair as many mode shapes between the FE-analysis and the system identification as possible. This will give us an idea of how accurate the model used in the FE-analysis is. The best pairings between the FE-analysis and the system identification are given in Table 7.

Table 7 shows that only 5 modes from the FEM have pairings with the SI with MAC over 0.5. Only 2 of them are of notable quality, mode 1 and 3 (from the SSI). The paired modes also do not match well with the natural frequencies. For all modes except the first global mode, the FEM modes have higher natural frequencies than the SI modes by 10% to 40%. This suggests that the FE-model is too stiff. This is

Table 7: Matching natural frequencies and mode shapes from FE-analysis and System Identification

FDD Mode	FEM Mode	FDD Natural Frequency	FEM Natural Frequency	Frequency Error	MAC Number
1	1	1.55	1.41	9.2%	0.7376
3	7	2.36	2.73	15.8%	0.6787
4	8	2.52	2.81	11.7%	0.5941
7	13	2.85	3.96	39.0%	0.5118
8	14	3.18	3.99	25.3%	0.5558

expected due to the fixed connections of the model. Mode 1 however is too flexible. This might hint at the bridge deck being too soft or having too much additional mass added to the model.

These results are poor. This might be due to the joints of the timber trusses having complicated dynamic behavior and thus having complicated dynamic responses. These complicated joints are simply modeled as fixed connections, and thus cannot describe the displacements at the top of the trusses of the mode shapes accurately.

6 Updated FE Model

For the purpose of Structural Health Monitoring, it is important that the model used accurately represents the dynamic behavior of the bridge. In order to increase the accuracy of the model, the model has been updated manually, such that it more accurately matches the results from the system identification. Structural changes are introduced to the model after updating.

6.1 Model Updating

For the manual model updating, the dynamic behavior is tuned by altering the stiffness of the bridge. This is done by creating new "dummy" materials and replacing the timber materials for selected parts of the bridge. The dummy materials retain the same mass as the original material but have an altered stiffness. These dummy materials are assigned to two parts in the model; the beams in the trusses and the bridge decks. The beams of the trusses are all replaced by dummy materials with stiffness multiplied by one factor. This applies also to the bridge decks, but with a separate factor. Only these two factors are iterated upon for each update.

The quality of each update of the model is determined by the frequency errors of the modes utilized for the update. Due to the low quality of the pairings in Table 7, the 1st horizontal mode and the 1st vertical mode are chosen for validating the quality of each update. For each iteration, the natural frequencies of the first horizontal and the first vertical modes determine how the stiffness will be altered in the next iteration. The frequency errors for the two modes are preferably low and similar. If the frequency errors are not similar, it hints to the model being too stiff or too flexible, instead of a balance. The MAC numbers of the modes from the updated models with the modes from the SSI are tracked, but not considered while updating the model. The model was iterated upon until further accuracy of the frequencies was not gained.

The settings used for each update, and the frequency errors for the 1st horizontal and the 1st vertical mode are given in Table 8. Update 0 is the original model. Frequency errors are in comparison to the SSI results.

Table 8: Update Settings

Update	Beam factor	Deck factor	Frequency errors horizontal	Frequency errors vertical
0	1.0	1.0	8.0%	8.8%
1	0.8	1.2	2.8%	5.1%
2	0.6	1.2	4.6%	1.2%
3	0.6	1.3	2.2%	2.7%
4	0.55	1.35	2.2%	1.3%
5	0.5	1.4	3.0%	0.2%
6	0.5	1.5	2.3%	0.9%
Final	0.7	1.2	3.6%	4.8%

Each update will be discussed separately, only considering the previous updates.

6.2 Update 1

The goal of the first update is to get a higher frequency for the first horizontal mode and a lower frequency for the first vertical mode. This is done by decreasing the stiffness of the timber beams in the trusses and increasing the stiffness in the bridge decks. For the beams, we multiply the original stiffness by 0.8 and for the decks, we multiply by 1.2.

The results from the comparison between the SSI and the updated FEM model are given in Table 9. Note that the MAC number given for the vertical mode is only for the vertical motion of the measurement points. The frequencies are now much closer for both modes. The MAC number for the first horizontal mode is notably higher. Even with the increased accuracy of the frequencies, the frequency error of the vertical mode is too high.

Table 9: Results from model update 1.

Mode	SSI Natural Frequency	FEM Natural Frequency	Difference in Natural Frequency	MAC-number of SSI and FEM
1st horizontal mode	1.53	1.49	2.8%	0.8102
1st vertical mode	3.48	3.76	5.1%	0.8978

6.3 Update 2

For the second update of the model, the results from the first update are considered. The first horizontal mode is very close in frequency, while the first vertical mode is further away. The goal of the second update is to further decrease the frequency of the first vertical mode and to observe the influence the stiffness of the truss has over the frequency of the first horizontal mode. For the beams, we multiply the original stiffness by 0.6 and for the decks, we multiply by 1.2.

The results from the comparison between the SSI and the updated FEM model are given in Table 10. Note that the MAC number given for the vertical mode is only for the vertical motion of the measurement points. The frequency for the vertical mode from the updated model is now closer to the frequency from the SSI. For the horizontal mode, the frequency is lower than for update 1. Thus decreased stiffness of the truss decreases the natural frequency of both modes, but the vertical mode is influenced more than the horizontal mode. The MAC numbers are functionally equivalent.

6.4 Update 3

For the third update of the model, the results from the first and second updates are considered. The goal of the third update is to further increase the frequency of the

Table 10: Results from model update 2.

SSI Mode	FEM Mode	SSI Natural Frequency	FEM Natural Frequency	Difference in Natural Frequency	MAC-number of SSI and FEM
1	1	1.53	1.46	4.6%	0.8149
10	13	3.48	3.52	1.2%	0.9173

first horizontal mode and to observe the influence the stiffness of the deck has over the frequency of the first vertical mode. For the beams, we multiply the original stiffness by 0.6 and for the decks, we multiply by 1.3.

The results from the comparison between the SSI and the updated FEM model are given in Table 11. Note that the MAC number given for the vertical mode is only for the vertical motion of the measurement points. The frequency for the horizontal mode from the updated model is now closer to the frequency from the SSI. For the vertical mode, the frequency is slightly worse than for update 2. Thus increased stiffness of the decks increases the natural frequency for both modes. The MAC numbers for both modes are slightly lower.

Table 11: Results from model update 3.

SSI Mode	FEM Mode	SSI Natural Frequency	FEM Natural Frequency	Difference in Natural Frequency	MAC-number of SSI and FEM
1	1	1.53	1.5	2.2%	0.7824
10	14	3.48	3.57	2.7%	0.8977

6.5 Update 4

For the fourth update of the model, the results from the previous updates are considered. The goal of the fourth update is to slightly increase the frequency of the first horizontal mode and slightly decrease the frequency of the first vertical mode. For the beams, we multiply the original stiffness by 0.55 and for the decks, we multiply by 1.35.

The results from the comparison between the SSI and the updated FEM model are given in Table 12. Note that the MAC number given for the vertical mode is only for the vertical motion of the measurement points. For this update, the vertical mode is slightly closer to the identified natural frequency, while the horizontal mode is unchanged in frequency. Now there is a significant drop in the quality of the MAC number.

Table 12: Results from model update 4.

SSI Mode	FEM Mode	SSI Natural Frequency	FEM Natural Frequency	Difference in Natural Frequency	MAC-number of SSI and FEM
1	1	1.53	1.5	2.2%	0.6788
10	14	3.48	3.53	1.3%	0.8476

6.6 Update 5

For the fifth update of the model, the results from the previous updates are considered. The goal of the fifth update is to slightly increase the frequency of the first horizontal mode and slightly decrease the frequency of the first vertical mode. For the beams, we multiply the original stiffness by 0.5 and for the decks, we multiply by 1.4.

The results from the comparison between the SSI and the updated FEM model are given in Table 13. Note that the MAC number given for the vertical mode is only for the vertical motion of the measurement points. For this model update, the natural frequencies of both modes are lower. The horizontal has a natural frequency further from the identified frequency and the vertical mode has a natural frequency practically identical to the identified frequency. The MAC numbers for both modes are much lower. The horizontal mode is now arguably not resembling the identified horizontal mode.

Table 13: Results from model update 5.

SSI Mode	FEM Mode	SSI Natural Frequency	FEM Natural Frequency	Difference in Natural Frequency	MAC-number of SSI and FEM
1	1	1.53	1.48	3.0%	0.5059
10	14	3.48	3.47	0.2%	0.7811

6.7 Update 6

For the sixth update of the model, the results from the previous updates are considered. The goal of the fifth update is to slightly increase the frequency of the first horizontal mode and allow a slight increase in the frequency of the first vertical mode. For the beams, we multiply the original stiffness by 0.5 and for the decks, we multiply by 1.5.

The results from the comparison between the SSI and the updated FEM model are given in Table 14. Note that the MAC number given for the vertical mode is only for the vertical motion of the measurement points. The frequency for the horizontal mode is slightly closer, while the frequency for the vertical is slightly further away.

They are both very close now. However, the MAC numbers are much lower than for update 5. The horizontal mode can no longer be said to represent the identified mode.

Table 14: Results from model update 6.

SSI Mode	FEM Mode	SSI Natural Frequency	FEM Natural Frequency	Frequency Error	MAC-number of SSI and FEM
1	1	1.53	1.49	2.3%	0.3922
10	14	3.48	3.51	0.9%	0.7502

6.8 Model Updating Review

For the final update, the results of the previous six updates are reviewed. Figure 17 displays the frequency error for both modes for each model update. In the plot, it is clear that the first update greatly improves the frequency error of the modes. All updates after improves one of the modes at the expense of the other mode, except for update 4, where the frequency error in the vertical mode is improved, while the frequency error for the horizontal mode is retained from update 3. Update 3 is the update where the frequency error is most similar for both modes with 2.2% and 2.7%.

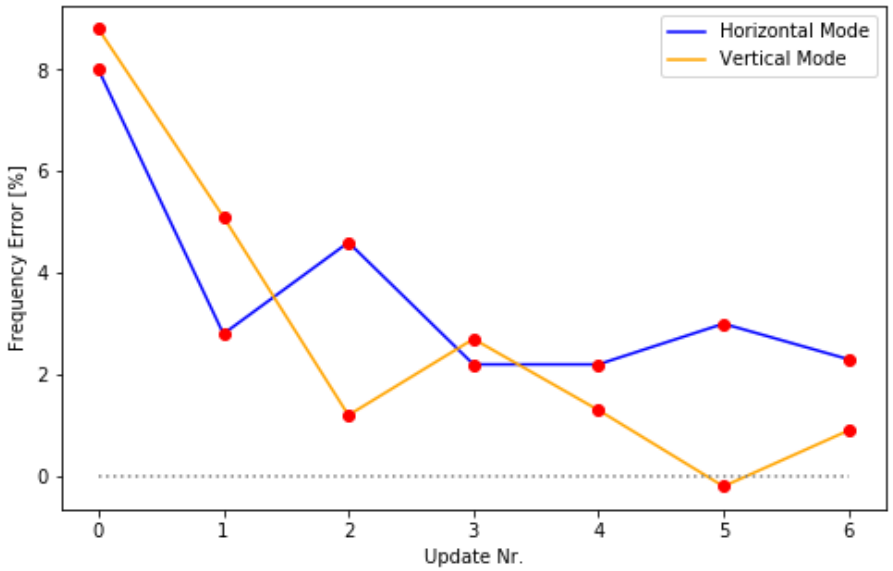

Figure 17: Frequency Errors for each model update.

Figure 18 displays the MAC numbers for both modes for each model update. In the graph, it is clear that the MAC number of the vertical mode decreases for each update. For the horizontal update, the MAC number increases for the first two updates and remains high for the first three updates. For both modes, the MAC numbers decrease significantly for each update after the third update.

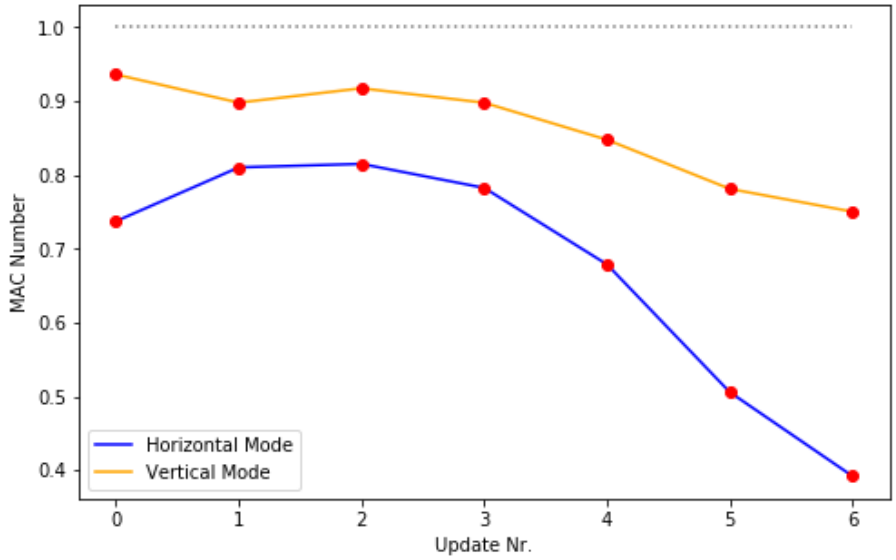

Figure 18: MAC Number for each model update.

6.9 Final Update

From the review of the model updating, these patterns emerged. The frequency error demonstrated only a marginal decrease from update 4 onwards, while the MAC number for the vertical mode consistently maintained a high and stable value throughout the initial three updates, indicating a reliable performance. Conversely, the MAC number for the horizontal mode showcased a similar high value during the first three updates, suggesting robust operational performance. To further optimize the system, a final update was designed to align settings between the initial two updates, aiming to achieve similar and minimized frequency errors for both vertical and horizontal modes while ensuring consistently high MAC numbers. This strategic adjustment sought to balance error rates between modes while sustaining high MAC numbers, potentially enhancing the dynamic performance of the FE model.

For the final model update the settings and results from update 1 are considered. As previously mentioned, the aim of the final update is to achieve similar and minimized frequency errors for both the vertical and the horizontal modes. This is attempted by lowering the stiffness of the beams in the truss slightly. This will greatly improve the frequency error of the vertical mode and slightly increase the frequency error of the horizontal mode, such that they are similar. For the beams, we multiply the original stiffness by 0.7 and for the decks, we multiply by 1.2.

The results from the comparison between the SSI and the updated FEM model are given in Table 15. Note that the MAC number given for the vertical mode is only for the vertical motion of the measurement points. The frequency error for the modes is now similar, but too high. The MAC numbers are now higher than for any other model for both modes.

Table 15: Results from the final model update.

SSI Mode	FEM Mode	SSI Natural Frequency	FEM Natural Frequency	Frequency Error	MAC-number of SSI and FEM
1	1	1.53	1.48	3.6%	0.8206
10	2	3.48	3.65	4.8%	0.9343

6.10 Best Model Update

To evaluate all the updates and determine the best candidate for further use, the frequency errors and the MAC numbers are evaluated. The best update will exhibit low frequency errors, that are not too dissimilar in size. It will also have high MAC numbers, suggesting that the model retains stiffness and mass similar to reality. Considering Figures 17 and 18, the best result is update 3 with frequency errors of 2.2% and 2.7%, and MAC numbers 0.7824 and 0.8977 for the horizontal and vertical mode respectively. Comparing the third update to the final update, the final update has higher frequency errors and higher MAC numbers. Since the main objective of the update is to increase the accuracy of the frequency while retaining high MAC numbers, the model from update 3 is chosen as the best model and will be used for further analysis.

In order to assess the completion of the goal, to decrease the frequency of all modes except for the 1st horizontal mode, the updated model is compared to the original model. 8 modes are identified visually in the ABAQUS CAE, and compared to each other. The comparison is displayed in Table 16. From the table, it is clear that the goal is met.

Table 16: Comparison between the original model and the updated model.

Mode	Original Natural Frequency	Updated Natural Frequency	Frequency Changes	MAC-number
1st horizontal mode	1.41	1.5	6.3%	0.7780
Southwest mode	1.83	1.6	-12.7%	0.8964
Northeast mode	1.9	1.66	-12.6%	0.9247
Northwest mode	2.14	1.88	-12.1%	0.9543
Southeast mode	2.24	1.97	-11.9%	0.9788
3rd horizontal mode	2.55	2.37	-7.1%	0.8471
3rd wall mode	3.09	2.65	-14.0%	0.7650
1st vertical mode	3.79	3.57	-5.6%	0.3678

The final factors for the stiffnesses are k=0.6 for the trusses and k=1.3 for the bridge deck. Reducing the stiffness of the trusses by 40% is a massive reduction. This is done to mimic the stiffness exhibited by the system identification results. Since the exaggerated stiffness of the trusses in the model is due to the fixed connections, the stiffness could alternatively be remedied by modeling the intersections of the

trusses as springs and updating the stiffness of the springs instead of the stiffness of the beams. This would likely give better results for the mode shapes of the updated model. The increase in stiffness of the bridge deck is surprising since the lowest density of asphalt was chosen for the additional mass on the bridge decks. However, the asphalt is modeled only as a mass without stiffness. There is some stiffness in asphalt especially as the temperature decreases. The insufficient stiffness of the bridge deck of the original model might be due to the lack of stiffness contribution from the asphalt.

In conclusion, the update with the best results regarding frequency errors without compromising the MAC numbers is update 3. The Frequency error is very low and similar, and the MAC numbers are within reasonable values for the two modes chosen for the update.

7 Damage Introduction

By introducing damage to the model, the dynamic behavior of the damaged model can be analyzed. Functions of certain parts, as well as consequences for damaging or loading them to failure, can be predicted.

7.1 Introducing Damage

Damages are introduced to the model by changing the stiffness of the "damaged" beam. To simulate such damage, the stiffness of that beam is reduced to 1% of the original stiffness. This is true for the first 4 damages. The 5th damage is changing a boundary condition from restricting motion in the across bridge direction and vertical direction, to only restricting motion in the vertical direction.

There are 5 damages that have been applied separately, meaning two damages do not appear in the same model. This is done because the probability of two damages appearing simultaneously is lower than for one at a time. There is also a large amount of possible damage combinations, that cannot be covered in this project. The damages are as follows:

1. Beam of upper truss
2. Beam of lower truss over support
3. Beam of support
4. Thin hanger
5. Boundary condition of support

The location of each damage is visualized in Figure 19. All damages are introduced at the southeast part of the bridge. These are chosen to capture a wide variety of structural damages to the bridge.

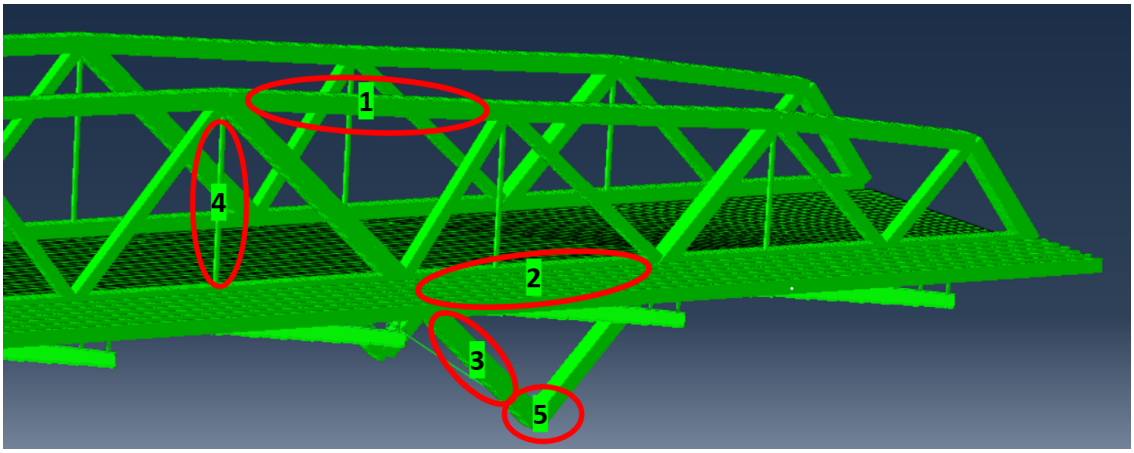

Figure 19: Damage locations.

To identify the impact of each damage on the dynamic behavior, 8 modes are identified, that appear for the undamaged model and all damages. All other modes

from the FE-analysis are excluded from this comparison. These 8 modes are as follows:

1. 1st horizontal mode
2. Southwest mode
3. Northeast mode
4. Northwest mode
5. Southeast mode
6. 3rd horizontal mode
7. 3rd wall mode
8. 1st vertical mode

Note that the modes of the corners of the walls (here 2, 3, 4, and 5) are not identified in the system identification. This is acceptable since the object of this exercise of introducing damage is to observe the consequences of the dynamic behavior.

Norsenga Bridge is a statically indeterminate structure. This means there is redundancy in the structure, and more than one beam to transfer any load through the structure. Removing one beam does not necessarily collapse the structure or alter the dynamic behavior of the structure. Owing to the modeling of the connections as fixed connections, the introduction of damages might have a lesser effect on the dynamic behavior of the structure than in reality, since the model is more structurally indeterminate than the real structure. Changes in the dynamic behavior from damages are expected to be greater in reality than the changes detected in this analysis. Note that for the modes of the corners of the walls, a larger effect on the southeast wall is expected compared to the other corners. This is because all damages are introduced in the southeast area.

7.2 Damage 1 - Beam of Upper Truss

Damage 1 is the damage of the beam of the upper truss marked in Figure 19.

The results from the comparison between the FE model with damage and the FE model without damage are given in Table 17. The frequency changes are small for the first 4 modes, but for the southeast mode, 3rd horizontal mode, and 3rd wall mode, the frequency change is notable. All frequencies are either lower or unchanged from the undamaged model. The MAC numbers are practically 1 for the 3 first modes. For the other modes, there is a notable change. Especially the 1st vertical mode shape is drastically changed, mostly in the horizontal behavior of the south truss. Note that for this damage, the 3rd wall mode is notably affected in both frequency and mode shape.

Since this damage largely affects the behavior of the south truss, an impact on the dynamic behavior was expected for all modes except the two not involving the south truss. These results are within expectations, with a few exceptions. The

first horizontal mode is practically unaffected. This might be due to the stiffness of the deck controlling the mode more than the stiffness of the trusses. The southwest mode is also not affected by the damage. This might be due to the artificial stiffness from the fixed connections, enabling the lower part of the truss to stiffen up the upper part. This might not be true for the real bridge. The notable change of the 3rd wall mode compared to the slightly less notable change of the 3rd horizontal mode, can be explained by the 3rd horizontal mode being more controlled by the stiffness of the north truss. The 3rd wall mode is more exposed to changes from this damage. All frequencies being lowered or unchanged is expected, since damaging the model is removing stiffness from the system, thus making it more flexible.

Table 17: Comparison of damage 1

Mode Shape	Undamaged Natural Frequency	Damaged Natural Frequency	Frequency Change	MAC-number
1st horizontal mode	1.50	1.49	0.2%	0.9976
Southwest mode	1.60	1.60	0.0%	0.9997
Northeast mode	1.66	1.66	0.1%	0.9999
Northwest mode	1.88	1.88	0.0%	0.9225
Southeast mode	1.97	1.87	5.0%	0.8976
3rd horizontal mode	2.37	2.31	2.4%	0.9380
3rd wall mode	2.65	2.55	4.0%	0.8088
1st vertical mode	3.57	3.54	0.9%	0.5016

7.3 Damage 2 - Beam of Lower Truss

Damage 2 is the damage of the beam of the lower truss over the support marked in Figure 19.

The results from the comparison between the FE model with damage and the FE model without damage are given in Table 18. Generally, the frequency changes are small and the MAC numbers are high. For the stiffness, there are two notable changes with the damage for the southeast mode and the 3rd horizontal mode. The only mode with a notable difference in mode shape is the 1st vertical mode, but mostly in the horizontal direction.

The damaged beam is between two stiff connections, that can transfer forces and retain stiffness in the absence of the damaged beam. This is exaggerated by the fixed connections of the model. This explains why there is so little change in the dynamic response. The third horizontal mode has decreased frequency likely because the bottom part of the truss is important to the stiffness, unlike the third wall mode, where the stiffness of the top of the trusses controls the frequency. The 1st vertical mode has horizontal motions that are unstable, and easily affected. Thus the lower MAC number is not unreasonable.

Table 18: Comparison of damage 2

Mode Shape	Undamaged Natural Frequency	Damaged Natural Frequency	Frequency Change	MAC-number
1st horizontal mode	1.50	1.49	0.2%	0.9986
Southwest mode	1.60	1.60	0.0%	1.0000
Northeast mode	1.66	1.66	0.1%	0.9998
Northwest mode	1.88	1.88	0.4%	0.9849
Southeast mode	1.97	1.92	2.8%	0.9826
3rd horizontal mode	2.37	2.3	2.8%	0.9808
3rd wall mode	2.65	2.65	0.3%	0.9947
1st vertical mode	3.57	3.56	0.3%	0.9240

7.4 Damage 3 - Beam of the Support

Damage 3 is the damage of the beam of the support marked in Figure 19.

The results from the comparison between the FE model with damage and the FE model without damage are given in Table 19. The notable changes in frequency and mode shapes are for the 1st horizontal mode, the 1st vertical mode, and the southeast mode. For the horizontal mode and vertical mode, the frequencies are slightly lower, but the mode shapes are greatly altered. For both modes, the great changes in the mode shape are in the horizontal direction. This is more notable for the horizontal mode shape. For the southeast mode, there is some change in the mode shape, but the impact on the frequency is the largest change. The frequency is lowered by over 11%.

The first horizontal mode and the first vertical mode are the two modes most reliant on the supports. The lowered frequencies for these modes and the altered mode shapes are within expectations. The southeast mode is heavily reliant on the southeast support specifically, which explains the great changes in the frequency for that mode.

Table 19: Comparison of damage 3

Mode Shape	Undamaged Natural Frequency	Damaged Natural Frequency	Frequency Change	MAC-number
1st horizontal mode	1.50	1.46	2.7%	0.8561
Southwest mode	1.60	1.60	0.0%	0.9983
Northeast mode	1.66	1.65	0.6%	0.9640
Northwest mode	1.88	1.88	0.0%	0.9968
Southeast mode	1.97	1.74	11.5%	0.9340
3rd horizontal mode	2.37	2.36	0.2%	0.9847
3rd wall mode	2.65	2.64	0.6%	0.9756
1st vertical mode	3.57	3.50	2.0%	0.7185

7.5 Damage 4 - Thin hanger

Damage 4 is the damage of the thin hanger marked in Figure 19.

The results from the comparison between the FE model with damage and the FE model without damage is given in Table 20. As expected, there is little effect on the dynamic behavior of the bridge. The most affected mode is the 3rd horizontal mode, where the frequency is reduced by 2%.

The role of the hanger is to connect the top of the truss to the beam supporting the main bridge deck, and also the pedestrian bridge deck. There are 16 hangers in total, 8 on each side of the road. This is very statically indeterminate and has a lot of redundancy. Damaging one hanger thus has little effect the the dynamic behavior of the bridge. The third horizontal mode has some vertical component, which is exaggerated by the reduced stiffness of the hanger, and therefore has reduced frequency.

Table 20: Comparison of damage 4

Mode Shape	Undamaged Natural Frequency	Damaged Natural Frequency	Frequency Change	MAC-number
1st horizontal mode	1.50	1.50	0.1%	1.0000
Southwest mode	1.60	1.60	0.0%	1.0000
Northeast mode	1.66	1.66	0.1%	1.0000
Northwest mode	1.88	1.88	0.1%	0.9989
Southeast mode	1.97	1.95	0.9%	0.9984
3rd horizontal mode	2.37	2.32	2.0%	0.9798
3rd wall mode	2.65	2.65	0.2%	0.9819
1st vertical mode	3.57	3.54	1.0%	0.9706

7.6 Damage 5 - Support (Boundary Condition)

Damage 5 is the damage of the support (boundary condition) marked in Figure 19.

The results from the comparison between the FE model with damage and the FE model without damage are given in Table 21. Note that for this damage the northeast mode is not detected. All modes are affected by this damage, except the first vertical mode, which was expected to not be influenced much. Both the southeast mode and the 3rd wall mode had a frequency reduction of about 3%. The MAC numbers for most nodes were reduced more than for the other damages.

These results show that the boundary conditions are greatly important to the dynamic behavior. The vertical mode is not affected since the boundary in the vertical direction is unchanged.

Table 21: Comparison of damage 5

Mode Shape	Undamaged Natural Frequency	Damaged Natural Frequency	Frequency Change	MAC-number
1st horizontal mode	1.50	1.51	0.6%	0.7488
Southwest mode	1.60	1.60	0.2%	0.9426
Northeast mode	1.66	-	-	-
Northwest mode	1.88	1.87	0.6%	0.7367
Southeast mode	1.97	1.91	3.1%	0.6812
3rd horizontal mode	2.37	2.35	0.8%	0.9048
3rd wall mode	2.65	2.58	2.7%	0.8832
1st vertical mode	3.57	3.57	0.0%	0.9996

7.7 Insights from Damages

By analyzing the results of all the damages introduced to the model, insights into the response of the structure can be gained. Figure 20 shows the frequency for each mode, for each damage. The dots on the thick lines are the frequencies of the damaged models, and the dotted lines behind are the natural frequencies of the undamaged model. The y-axis is each damage, numbered as in the descriptions. The greatest frequency changes are observed for the last 4 modes. These modes are not affected equally for all damages. The 3 wall corner modes that are not in the southeast have almost no impact on any damage. The mode of the southeast corner has notable frequency changes for most damages, except damage 4 (the thin hanger). Using this knowledge, by analyzing the response of each mode, it is possible to locate the general location of the damage, and possibly what type of damage it is. This requires great precision in the dynamic analysis.

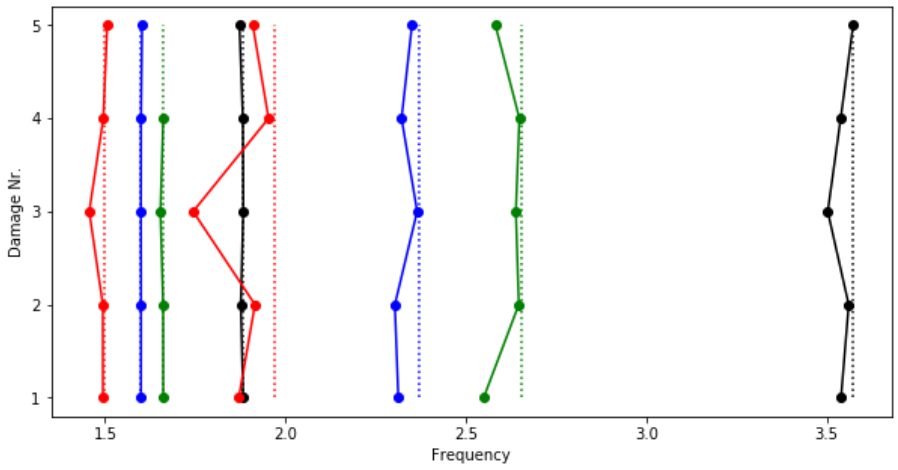

Figure 20: Plot of the frequencies for each mode for each damage.

The main insight gained on the impact of damages on the system dynamic response is that for most damages and most modes, changes in frequency are small. There

are also small changes for the MAC numbers, but several modes have reduced MAC numbers to 0.9 and below. These changes might be hard to detect in system identification since frequencies and MAC numbers change between recordings to that of a damaged model. One sign of damage is that all natural frequencies are either reduced or unchanged. However, it is necessary to analyze more than frequency changes to successfully carry out structural health monitoring of Norsenga Bridge.

8 Conclusion

In this thesis, the system identification of the Norsenga Bridge has been successful in acquiring natural frequencies and mode shapes for many low-order modes. When compared to the FE model created for this work, only the first horizontal mode shape has a relatively high MAC number. For the first horizontal mode, the natural frequency from the FE model is lower than the respective experimental natural frequency. For other modes, the numerical natural frequencies are higher than their experimental counterparts. Consequently, a series of manual updates were executed on the FE model, by adjusting parameters to gradually reduce the stiffness of the truss beams while augmenting the bridge stiffness of the deck. The primary objective was twofold: to increase the frequency of the initial horizontal bending mode, primarily reliant on the deck's stiffness, and to diminish the frequencies of the other identified modes, predominantly associated with the buckling motion of the trusses, and therefore heavily contingent on their stiffness. Practically, the decrease in the stiffness of the beams in the trusses makes up for overly stiff modeling of the joints. On the other hand, the increase in the stiffness of the bridge deck makes up for modeling the asphalt as a mere dead load with no stiffness. The result of the updating is a model with frequency errors of 2.2% and 2.7% instead of 8% and 8.8% for the first horizontal mode and the first vertical mode, respectively. Nevertheless, concerning mode shapes, the model continues to exhibit an unimpressive correlation with the experimental data, despite updates. One significant source of discrepancy could be attributed to the modeling assumption of fixed connections at the joints. Specifically, this assumption significantly influences the movement of the upper nodes of the trusses along the bridge's width, thus exerting a pronounced effect on the MAC. In order to achieve better matching between numerical and experimental responses, it is advisable to model the joints with rotational spring elements, to allow for greater rotational freedom.

Finally, using the updated model, damages were introduced. The numerical results show that the effects of damages on the dynamic behavior are mostly small and could therefore prove challenging to detect by SHM techniques that rely on modal features. However, it was noticed how distinct damage scenarios exhibit varied effects across different modes, amplifying the potential for detecting and possibly locating specific areas of damage based on their mode-specific responses.

References

[1] S. Vegvesen, "Norsenga bru på e16 i kongsvinger gjenåpnes torsdag." https://www.vegvesen.no/om-oss/presse/aktuelt/2022/09/norsenga-bru-pa-e16-i-kongsvinger-gjenapnes-torsdag/, 2022. Read 18.10.2023.

[2] V. Goldfine, "Dynamic properties of hell bridge." Not published, 2022.

[3] D. Newland, *An Introduction to Random Virations, Spectral Wavelet Analysis*. New York, USA: Dover, 3 ed., 1975. Chapter 3 and 5.

[4] Øyvind W. Petersen, "Example 6-3: System identification." https://github.com/oiseth/TKT4108StructuralDynamics2/blob/main/python/jupyterNotebooks/Example%206_3%20System%20identification.ipynb, 2022. Read 22.12.2023.

[5] K. A. Kvåle, "Covariance-driven stochastic subspace identification of an end-supported pontoon bridge under varying environmental conditions." https://doi.org/10.1007/978-3-319-54777-0_14, 2017. Read 20.12.2023.

[6] R. J. Allemang, *The Modal Assurance Criterion - Twenty Years of Use and Abuse*. University of Cincinnati, 2003.

[7] J. E. Mottershead and M. I. Friswell, *Finite Element Model Updating in Structural Dynamics*. Dordrecht, Netherlands: Springer Dordrecht, 1 ed., 1995. Chapter 8.

[8] J. E. Mottershead and M. I. Friswell, *Model Updating In Structural Dynamics: A Survey*. Massachusetts, USA: Academic Press, 1 ed., 1993. Chapter 1 and 2.

[9] B. T. Svendsen, "A hybrid structural health monitoring approach for damage detection in steel bridges under simulated environmental conditions using numerical and experimental data." https://doi.org/10.1177/14759217221098998, 2017. Read 21.12.2023.

[10] DEWESoft, "Iolite® 3xmems." https://dewesoft.com/products/iolitei-3xmems, 2022. Read 22.12.2023.

[11] K. A. Kvåle, "knutankv." https://doi.org/10.5281/zenodo.10277112, 2023. Read 23.12.2023.

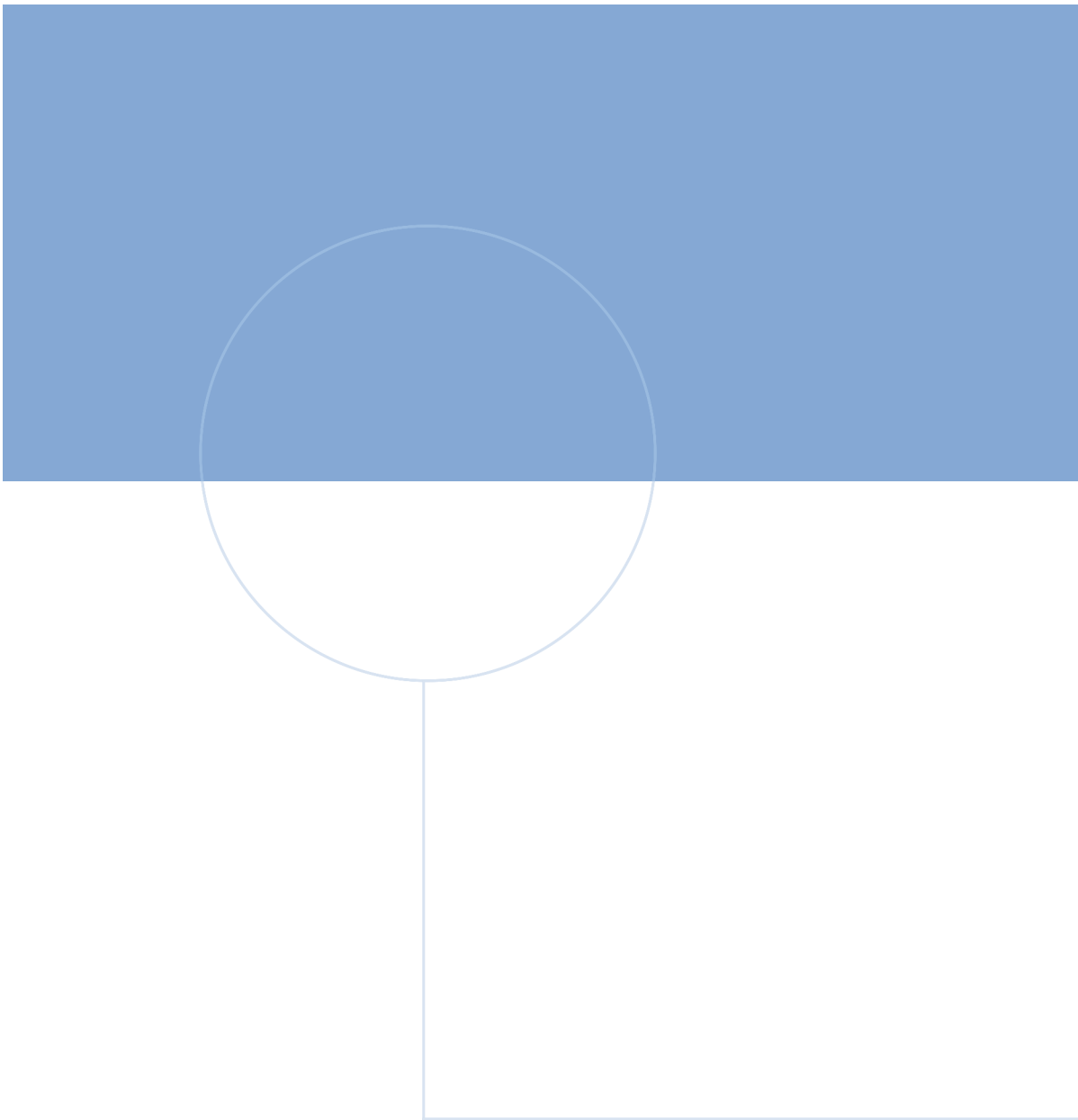

NTNU

Norwegian University of
Science and Technology